

# Charge Ordering in Organic ET Compounds

Hitoshi SEO\*

*Institute for Solid State Physics, University of Tokyo, Minato-ku, Tokyo 106-8666, Japan*

(Received )

The charge ordering phenomena in quasi two-dimensional 1/4-filled organic compounds  $(\text{ET})_2X$  ( $\text{ET}=\text{BEDT-TTF}$ ) are investigated theoretically for the  $\theta$  and  $\alpha$ -type structures, based on the Hartree approximation for the extended Hubbard models with both on-site and intersite Coulomb interactions. It is found that charge ordered states of stripe-type are stabilized for the relevant values of Coulomb energies, while the spatial pattern of the stripes sensitively depends on the anisotropy of the models. By comparing the results of calculations with the experimental facts, where the effects of quantum fluctuation is incorporated by mapping the stripe-type charge ordered states to the  $S = 1/2$  Heisenberg Hamiltonians, the actual charge patterns in the insulating phases of  $\theta$ -( $\text{ET})_2MM'(\text{SCN})_4$  and  $\alpha$ -( $\text{ET})_2\text{I}_3$  are deduced. Furthermore, to obtain a unified view among the  $\theta$ ,  $\alpha$  and  $\kappa$ -( $\text{ET})_2X$  families, the stability of the charge ordered state in competition with the dimeric antiferromagnetic state viewed as the Mott insulating state, which is typically realized in  $\kappa$ -type compounds, and with the paramagnetic metallic state, is also pursued by extracting essential parameters.

KEYWORDS: charge ordering, organic conductors, BEDT-TTF, extended Hubbard model, Hartree approximation.

## §1. Introduction

The family of quasi two-dimensional (2D) organic conductors  $(\text{ET})_2X$  ( $\text{ET}=\text{BEDT-TTF}$ ) is known to exhibit a variety of interesting electronic properties.<sup>1)</sup> Their structure consists of alternating layers of anionic  $X^-$  with the closed shell, and cationic  $\text{ET}^{1/2+}$  whose  $\pi$ -band is 3/4-filled (1/4-filled in terms of holes) if all the ET molecules are equivalent. The variety in physical properties reflects that of spatial arrangements of ET molecules in the layer, which are classified by greek characters such as  $\kappa$ ,  $\alpha$ ,  $\theta$ ,  $\beta$ , etc., together with the rather strong mutual Coulomb interaction among  $\pi$ -electrons.<sup>2)</sup> Theoretical studies of Kino and Fukuyama<sup>3,4,5,6)</sup> (KF) developed a systematic way to understand the diversity in their ground state properties by taking into account the explicit anisotropy of the transfer integrals between ET molecules for each compound, and by

---

\* E-mail: hseo@swan.issp.u-tokyo.ac.jp

mean-field (MF) calculations treating the on-site Coulomb interaction  $U$  within the Hartree-Fock approximation.

By studying the structure of  $\kappa$ -(ET) $_2X$  where the intradimer transfer integral is twice larger than the others,<sup>7)</sup> and by varying the degree of the dimerization, KF have investigated the stability of the insulating state with antiferromagnetic (AF) ordering between dimers, which is called the dimeric AF state.<sup>4)</sup> This state is stable when the dimerization in the ET layer is strong, since the electron correlation results in a Mott insulating state due to the 1/2-filled  $\pi$ -band,<sup>8,9)</sup> as has been first argued by Tokura.<sup>10)</sup>

Another interesting conclusion of KF is that the  $\alpha$ -type compounds show tendency toward an insulating state with charge ordering (CO) (charge transfer in their notation).<sup>3)</sup> Experimentally,  $\alpha$ -(ET) $_2I_3$  shows a metal-insulator (MI) transition at  $T_{MI}=135$  K<sup>11)</sup> at ambient pressure, and by applying pressure this  $T_{MI}$  is suppressed.<sup>12)</sup> The magnetic susceptibility shows a sharp drop below  $T_{MI}$  indicating a non-magnetic ground state with a spin gap.<sup>13)</sup> A bond length analysis<sup>14)</sup> as well as an IR absorption experiment<sup>15)</sup> in this compound suggest charge disproportionation among ET molecules, though the suggested spatial patterns of charge disproportionation are different from each other. The Hartree-Fock calculations by KF for the structure of  $\alpha$ -(ET) $_2I_3$  show CO between the stacks I and II, which are the two crystallographically inequivalent columns as shown in Fig. 1(a). The actual pattern of CO as well as the nature of the phase transition in this compound is still an open problem. Recently some suggestions have been made that the ground state of another class of  $\alpha$ -phase,  $\alpha$ -(ET) $_2M\text{Hg}(\text{SCN})_4$  for  $M=\text{K, Rb, and Tl}$ , which are isostructural to  $\alpha$ -(ET) $_2I_3$  (see Fig. 1(a)), may also be a charge disproportionated state<sup>16)</sup> rather than the so far believed spin-density-wave (SDW) state due to the nesting of Fermi surface.<sup>5,17)</sup>

Recently such CO has been directly observed in NMR measurements by Miyagawa *et al*<sup>19)</sup> and by Chiba *et al*<sup>20)</sup> in a member of another polytype  $\theta$ -(ET) $_2X$ . A series of these compounds,  $\theta$ -(ET) $_2MM'(\text{SCN})_4$  ( $M=\text{Rb, Tl, Cs, } M'=\text{Co, Zn}$ ), has been synthesized by H. Mori *et al*,<sup>21)</sup> who have proposed that the properties of  $\theta$ -phase can be summarized in one phase diagram, where the horizontal axis is the dihedral angle,  $\phi$ ,<sup>22)</sup> between the molecular planes, which is different for each compound. It has been argued by Takahashi and Nakumara<sup>23)</sup> that a phase diagram, a slightly modified version of ref. 21, can be drawn as shown in Fig. 2, since it has been realized by experiments that among the above series, located in the region of  $100^\circ \lesssim \phi \lesssim 140^\circ$ , there exist compounds with two different types of structures, the usually called  $\theta$ -type one, as shown in Fig. 1(b), and another one with slight dimerization along the  $c$ -axis, as shown in Fig. 1(c), which we call here  $\theta_d$ -type to make distinction. The electronic properties of these two phases are distinct to each other. The compounds in the  $\theta$ -phase which exist in the left side of the phase diagram ( $\phi \lesssim 110^\circ$ ) are metallic at room temperature, and show a minimum in their resistivities at  $T_\rho = 50 - 100$  K and by applying pressure  $T_\rho$  increases,<sup>21)</sup> except in  $\theta$ -(ET) $_2I_3$  exhibiting superconducting behavior

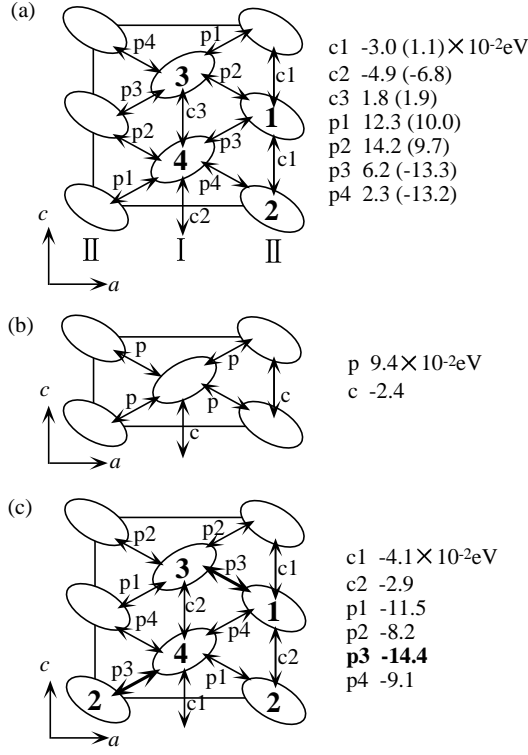


Fig. 1. Schematic representation of the structures in the donor plane for  $(\text{ET})_2X$  compounds;  $\alpha$ -type (a),  $\theta$ -type (b) and  $\theta_d$ -type (c) (see the text for the notation of  $\theta_d$ ). ET molecules are drawn as ellipses, and the intermolecular transfer integrals are given by  $t = Es$  with  $E = -10$  eV, where the overlap integrals  $s$  are for  $\alpha$ -( $\text{ET})_2\text{I}_3$ <sup>18)</sup> (a) where the indices are modified from those in ref. 18 as  $a1 - a3 \rightarrow c1 - c3$  and  $b1 - b4 \rightarrow p1 - p4$ , (those corresponding to  $\alpha$ -( $\text{ET})_2\text{NH}_4\text{Hg}(\text{SCN})_4$  are also shown in the parentheses of (a)<sup>17)</sup>),  $\theta$ -( $\text{ET})_2\text{CsZn}(\text{SCN})_4$ <sup>21)</sup> (b) and  $\theta$ -( $\text{ET})_2\text{RbCo}(\text{SCN})_4$ <sup>21)</sup> (c).

below 3.6 K.<sup>24)</sup> Their magnetic susceptibilities show Curie-like behavior with no sign of magnetic order down to low temperatures.<sup>25,26)</sup> On the other hand, in the  $\theta_d$ -phase located in the right side of the phase diagram ( $\phi \gtrsim 110^\circ$ ), the resistivity shows an insulating behavior ( $d\rho/dT < 0$ )<sup>21,27)</sup> below room temperature and its magnetic susceptibility follows that of the 1D Heisenberg model ( $J \sim 160$  K for  $\theta_d$ -( $\text{ET})_2\text{RbZn}(\text{SCN})_4$ ) but exhibits a spin gap behavior at low temperature in some compounds.<sup>21,27,28)</sup> This spin gap behavior is also confirmed by  $^{13}\text{C}$ -NMR measurements.<sup>19,26)</sup> The CO was recently found in the  $\theta_d$ -phase of  $(\text{ET})_2\text{RbZn}(\text{SCN})_4$ <sup>19,20)</sup> which is located in the critical region between the two phases.<sup>26)</sup> At room temperature it has  $\theta$ -type structure, and upon cooling the sample slowly, the resistivity suddenly increases at  $T_{\text{str}} = 195$  K where it is believed that a structural phase transition takes place from  $\theta$  to  $\theta_d$ -type structure, while this structural phase transition is absent if the sample is cooled rapidly so that the  $\theta$ -type structure is maintained down

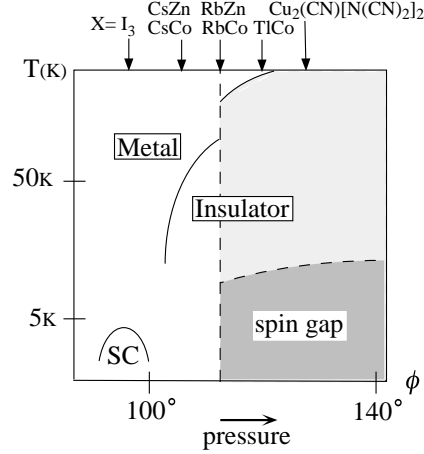


Fig. 2. Schematic phase diagram of  $\theta$ -(ET) $_2$ X deduced from experiments, on the plane of dihedral angle ( $\phi$ ) and temperature (T).<sup>21,23)</sup> The effect of pressure is indicated by the arrow, and SC denote the superconducting phase. The colored area show the  $\theta_d$ -phase, while the other is the  $\theta$ -phase. The locations of ambient pressure are shown for examples of anions X, where  $X = MM'(\text{SCN})_4$  ( $M=\text{Rb, Tl, Cs}$ ,  $M'=\text{Co, Zn}$ ) is abbreviated as  $MM'$ .

to low temperatures. In the slowly cooled case, the  $^{13}\text{C}$ -NMR measurements show the existence of the charge disproportionation among ET molecules in the  $\theta_d$ -phase below  $T_{\text{str}}$ , i.e. the occurrence of a CO state.<sup>19,20)</sup>

As for theoretical studies on the CO phenomena in 1/4-filled organic conductors, most are limited to those in one-dimensional (1D) cases. The effects of *intersite* Coulomb interactions  $V_{i,j}$  in such quasi 1D systems have been studied from early days<sup>29)</sup> and it is known that  $V_{i,j}$  makes the system toward the  $4k_F$  CDW, i.e. CO, which is actually observed experimentally in (DI-DCNQI) $_2\text{Ag}$ .<sup>30)</sup> In the case of (TMTTF) $_2$ X the interplay between this  $V_{i,j}$  and the on-site Coulomb energy  $U$  together with the intrinsic dimerization give rise to a intermediated state between the dimeric AF state and the CO state,<sup>31)</sup> and in the cases of  $X=\text{Br}$  and  $\text{SCN}$  experiments suggest the existence of the expected charge disproportionation.<sup>32,33)</sup> As regards the 2D case, the importance of this  $V_{i,j}$  has been clarified recently in a 1/4-filled transition metal oxide  $\text{NaV}_2\text{O}_5$ , where a similar interplay between  $U$ ,  $V_{i,j}$  and the dimerization is present, and its ground state is proposed to be a peculiar type of CO state due to this  $V_{i,j}$ .<sup>34)</sup> As for the organic systems, the calculations without  $V_{i,j}$  for  $\theta_d$ -type structure predict the ground state to be Mott insulating state,<sup>35)</sup> inconsistent with the existence of CO disclosed by the experiments mentioned above. Thus, studies including  $V_{i,j}$  are needed to understand CO phenomena in the above 2D organic conductors, although CO itself has already been suggested in  $\alpha$ -type structures from the Hartree-Fock calculations by KF.<sup>3)</sup>

The actual values of this  $V_{i,j}$  in ET compounds are expected to be relatively large due to the

fact that the wave function of the MO in molecular conductors is rather extended, so  $U$  is expected to be suppressed so that to be comparable to neighboring  $V_{i,j}$ . Furthermore, the screening of  $V_{i,j}$  cannot be expected in ET compounds for the HOMO  $\pi$ -band which is separated from the other bands, as in the transition metals where the  $s$ -band screens the long range Coulomb interactions between the  $d$ -electrons. Actually several calculations for organic compounds estimate the nearest-neighbor Coulomb energy  $V$  to be 20 – 50% of  $U$ .<sup>36,37)</sup> In this paper we consider the value of  $U$  on ET molecule to be approximately 0.7 eV, which is derived from the analysis of NMR data of  $\kappa$ -(ET)<sub>2</sub>Cu[N(CN)<sub>2</sub>]Br based on random phase approximation,<sup>38)</sup> and the values of the neighboring  $V_{i,j}$  to be 0.15 – 0.35 eV, adopting the ratio  $V_{i,j}/U = 0.2 - 0.5$  from the above calculations.

In this paper, we investigate the effect of both the on-site and the intersite Coulomb interactions on the electronic states in (ET)<sub>2</sub> $X$  and our goal is not only to understand the electronic properties of the  $\theta$ ,  $\theta_d$  and  $\alpha$ -phases but also to provide a unified view on the variety of ground states of this family. In §2 the interrelationship between the  $\theta$ ,  $\theta_d$ ,  $\alpha$  and  $\kappa$ -type structures based on a simplified model is explained together with the formulation of the MF calculations based on the work of KF,<sup>6)</sup> and also an explanation of the CO states of stripe-type, which is an analogy to the phenomena first found in Nickel oxides,<sup>39)</sup> is given. The results of calculations for each type of structure, i.e.  $\theta$ ,  $\theta_d$  and  $\alpha$ -type, are shown in §3, together with the results for the simplified model. The relevance to the actual compounds is discussed in §4 by comparing them with the experiments and a unified view on the electronic properties of (ET)<sub>2</sub> $X$  is given. §5 is devoted to the summary and the conclusion. In the following sections we call the  $\alpha$ -type structures with transfer integrals corresponding to  $\alpha$ -(ET)<sub>2</sub>I<sub>3</sub> and  $\alpha$ -(ET)<sub>2</sub>MHg(SCN)<sub>4</sub>, as  $\alpha$ I<sub>3</sub>-type and  $\alpha$ MHg-type, respectively, for abbreviation.

## §2. Model and Formulation of Mean Field Calculations

### 2.1 Interrelationship among different polytypes of (ET)<sub>2</sub> $X$

It is useful to compare the structural features and the band structures of different polytypes, which has been carried out by KF<sup>5,6)</sup> who pursued the interrelationship between  $\kappa$ ,  $\alpha$ I<sub>3</sub> and  $\alpha$ MHg-type structures on the plane of two key ingredients, i.e. the degree of dimerization and that of band overlap. Here we review their framework and also find out where the  $\theta$  and  $\theta_d$ -type structures are located, by referring a simplified model described in Fig. 3. This model has been introduced by KF in order to unify their results for the  $\alpha$ -type and  $\kappa$ -type structures, yet they have not performed actual calculation on this simplified model.

In Fig. 4, the band structures of  $\theta$ -type (a),  $\theta_d$  and  $\kappa$ -type (b), and  $\alpha$ I<sub>3</sub> and  $\alpha$ MHg-type<sup>40)</sup> (c) are shown, respectively. It can be seen in Fig. 4(a) that the energy band of  $\theta$ -type compounds is simply 3/4-filled, while in Fig. 4(b) for  $\theta_d$  and  $\kappa$ -types the upper two bands and the lower two bands are split due to the dimerization. Especially, the band of  $\kappa$ -phase has a clear dimerization gap while the splitting is not appreciable in the  $\theta_d$ -phase, since the relative value of the interdimer

transfer integral compared to other transfer integrals, i.e. the degree of dimerization, is quite larger in the  $\kappa$ -type than in the  $\theta_d$ -type; the interdimer transfer integral in the  $\kappa$ -type structure is 0.257 eV ( $t_{b1}$  in Fig. 7) which is twice larger than the other transfer integrals while the one for the  $\theta_d$ -type structure is 0.144 eV ( $t_{p3}$  in Fig. 1(c)), slightly larger than the other transfer integrals in the transeverse direction,  $t_{p1}$ ,  $t_{p2}$  and  $t_{p4}$ . The difference among the two  $\alpha$ -type compounds has been clarified in the work of KF,<sup>5,6)</sup> who indicated that this is the degree of the band overlap resulting from the difference in the absolute value of the transfer integral  $t_{p4}$  as shown in Fig. 1(a). The relatively small value of  $|t_{p4}|$  in the  $\alpha I_3$ -type structure results in the small band overlap, while the energy bands for the  $\alpha M Hg$ -type structure has larger overlap due to the larger value of  $|t_{p4}|$ , as seen in Fig. 4(c).

It turns out that the simplified model in Fig. 3 is also an effective model for these  $\kappa$  and  $\theta_d$ -type structures by varying  $t_{p1}$ , and for  $\alpha$ -type structures by varying  $t_{p4}$ , as can be seen in the following. The model in Fig. 3(a) is the  $\theta$ -type structure which has the inversion as well as the spiral symmetry. If the absolute value of  $t_{p1}$  in Fig. 3(b) is increased, the inversion symmetry is lost, and only the spiral symmetry is retained, which corresponds to the situation of  $\kappa$  and  $\theta_d$ -type structures. If  $t_{p4}$  in Fig. 3(b) is varied, then only the inversion symmetry is retained, which is the situation of  $\alpha$ -type structures. In Fig. 5, the band structures for the model in Fig. 3(b) are shown for different parameters, which are  $t_a = 0.01$  eV,  $t_{b4} = t_b = 0.1$  eV and  $t_{b1} = 0.1, 0.2, 0.3$  eV (a), and  $t_a = 0.01$  eV,  $t_{b1} = t_b = 0.1$  eV and  $t_{b4} = 0.1, 0.05, 0.0$  eV (b). The general features seen in Figs. 4 (b) and (c) are well reproduced in Figs. 5 (a) and (b), respectively. Thus the calculations on this simplified model will provide us the idea of a unified view of the  $(ET)_2X$  family. The interrelationship between the phases can be summarized in Fig. 6, which is similar to the corresponding figure in ref. 5 but the locations of the  $\theta$  and  $\theta_d$ -phases beeing added.

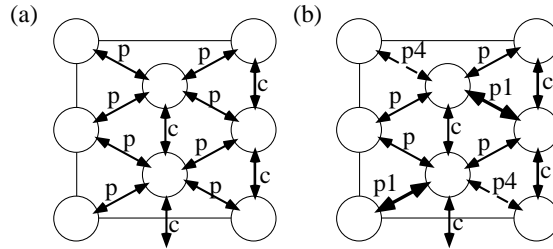


Fig. 3. A simplified model for  $(ET)_2X$  introduced by KF.<sup>6)</sup> The circles and the arrows represent the ET molecules and the intermolecular transfer integrals, respectively.

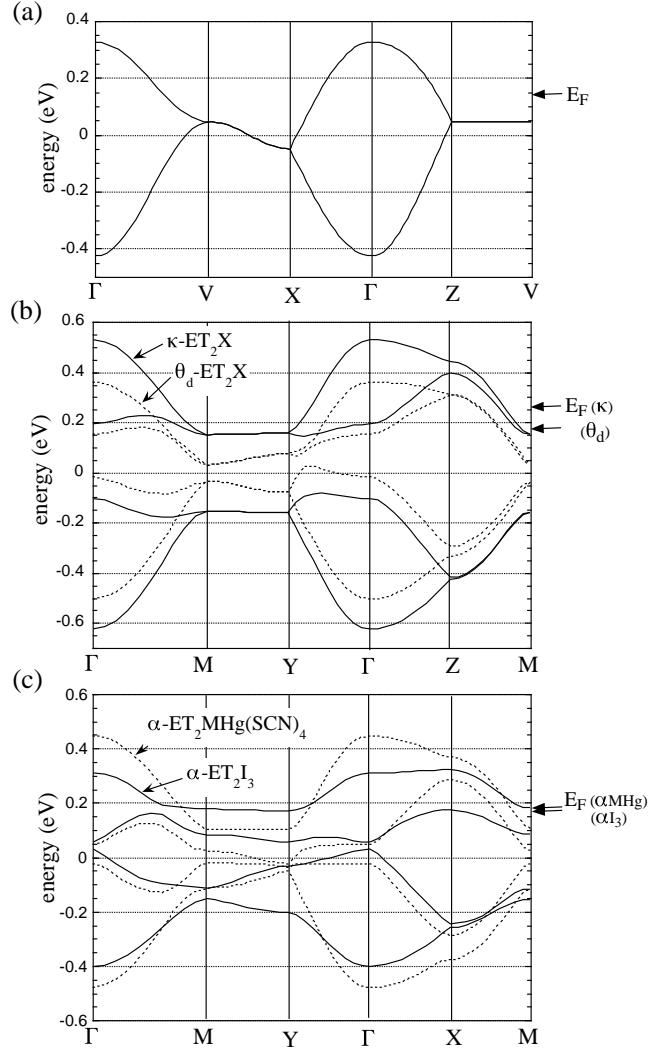


Fig. 4. The tight binding band structures of  $\theta$ -type (a),  $\theta_d$ -type and  $\kappa$ -type (b),  $\alpha I_3$ -type and  $\alpha MHg$ -type<sup>22)</sup>(c) structures, where the transfer integrals are taken from those in Fig. 1. The fermi energy for each case is also shown.

## 2.2 Formulation

2D layer of ET molecules is considered by taking into account the transfer integrals between them and the mutual Coulomb interaction among electrons. In this work the treatment of KF is basically followed,<sup>6)</sup> but here the intersite Coulomb interactions are also included. Thus our Hamiltonian is an extended Hubbard one, which is as follows;

$$H = \sum_{\langle i,j \rangle} \sum_{\sigma} \left( t_{i,j} a_{i\sigma}^{\dagger} a_{j\sigma} + h.c. \right)$$

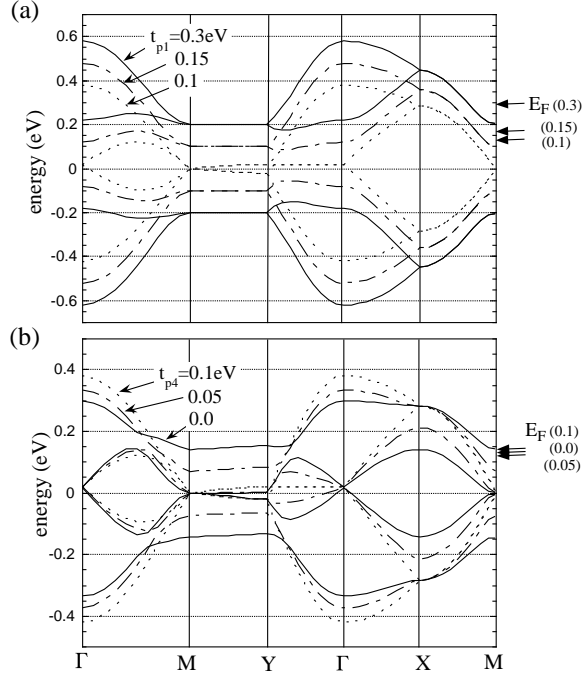


Fig. 5. The band structures for the simplified model shown in Fig. 3 (b).  $t_c$  and  $t_p$  are fixed at 0.01 eV and 0.1 eV, respectively. The band structures for the case of  $t_{p4} = t_p$  varying  $t_{p1} = 0.1, 0.15, 0.20$  eV (a) and for the case of  $t_{p1} = t_p$  and  $t_{p4} = 0.1, 0.05, 0.0$  eV (b) are shown together with the fermi energy for each case.

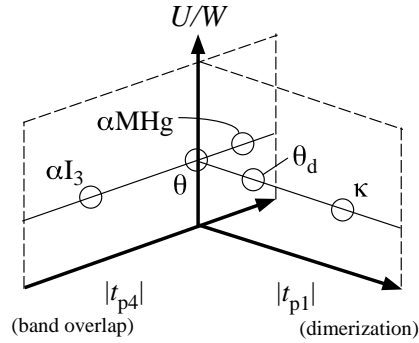


Fig. 6. Interrelationship between different types of structures for  $(\text{ET})_2\text{X}$ , schematically shown in the plane of  $t_{p1}$  and  $t_{p4}$ , which are the transfer integrals in the model structure described in the inset (identical to the one in Fig. 3(b)), which controls the degree of dimerization and band overlap, respectively.



$$+ \sum_i U n_{i\uparrow} n_{i\downarrow} + \sum_{\langle i,j \rangle} V_{i,j} n_i n_j, \quad (1)$$

where  $\langle i, j \rangle$  denotes the neighboring site pair,  $\sigma$  is the spin index which takes  $\uparrow$  and  $\downarrow$ ,  $n_{i\sigma}$  and  $a_{i\sigma}^\dagger$  ( $a_{i\sigma}$ ) denote the number operator and the creation (annihilation) operator for the electron of spin  $\sigma$  at the  $i$ th site, respectively, and  $n_i = n_{i\uparrow} + n_{i\downarrow}$ .

The Coulomb interactions  $U$ ,  $V_{i,j}$  are treated within the MF approximation in a manner similar to that in refs. 3-6,31,34;

$$\begin{aligned} n_{i\uparrow} n_{i\downarrow} &\rightarrow \langle n_{i\uparrow} \rangle n_{i\downarrow} + n_{i\uparrow} \langle n_{i\downarrow} \rangle - \langle n_{i\uparrow} \rangle \langle n_{i\downarrow} \rangle \\ n_i n_j &\rightarrow \langle n_i \rangle n_j + n_i \langle n_j \rangle - \langle n_i \rangle \langle n_j \rangle, \end{aligned} \quad (2)$$

which corresponds to the Hartree approximation. The MF Hamiltonian in  $k$ -space is given by

$$H^{\text{MF}} = \sum_{k\sigma} \begin{pmatrix} a_{1k\sigma} \\ a_{2k\sigma} \\ \vdots \\ a_{mk\sigma} \end{pmatrix}^\dagger \left[ h_0 + U \begin{pmatrix} n_{1\bar{\sigma}} & & 0 \\ & n_{2\bar{\sigma}} & \\ & & \ddots \\ 0 & & & n_{m\bar{\sigma}} \end{pmatrix} + h_V \right] \begin{pmatrix} a_{1k\sigma} \\ a_{2k\sigma} \\ \vdots \\ a_{mk\sigma} \end{pmatrix}, \quad (3)$$

where  $h_0$  and  $h_V$  denote the matrices for the kinetic energy term and the intersite Coulomb interaction term, respectively. The actual form of these matrices depends on each structure and unit cell size whose examples are shown in §2.3.

The crystallographic unit cell in the layer for the  $\theta$ -type structure is approximated as rectangle with  $a = 2c$  and those for the  $\theta_d$  and  $\alpha$ -type structures as square.

Self-consistent solutions are searched for at  $T = 0$  with the average electron density being fixed at 1.5 per ET site by considering several unit cell sizes and their energies are compared so that the ground state can be decided. The solutions where the net magnetic moment of the whole system is finite, i.e. ferro/ferrimagnetic solutions are neglected, as in the work of KF, since the stability of these states, if it occurs, can be thought to be the artifact of the approximation. The total energy  $\mathcal{E}$  is calculated as

$$\begin{aligned} \mathcal{E} &= \frac{1}{N_{\text{cell}}} \sum_{lk\sigma} \epsilon_{lk\sigma} n_F(\epsilon_{lk\sigma}) \\ &\quad - \sum_i U \langle n_{i\uparrow} \rangle \langle n_{i\downarrow} \rangle - \sum_{\langle i,j \rangle} V_{i,j} \langle n_i \rangle \langle n_j \rangle, \end{aligned} \quad (4)$$

where  $N_{\text{cell}}$  is the total number of the cells,  $\epsilon_{lk\sigma}$  is the  $l$ th eigenvalue of the  $m \times m$  Hamiltonian matrix in eq. 3 at each  $k$  and  $n_F(\epsilon)$  is the Fermi distribution function.

The intersite Coulomb interactions we consider are taken along the bonds with transfer integrals in Fig. 1, i.e. those between the neighboring ETs. For simplification only two kinds of values are considered: the intersite Coulomb energy along the stacking direction  $V_c$  which is the one between parallel molecules, and along the bonds in the transverse directions  $V_p$  which is the one between

molecules with dihedral angle  $\phi$ . In the actual compounds, the values of intermolecular Coulomb energy should be different for the bonds with different transfer integral since the configurations between pair of molecules are different. So the above model with only  $V_c$  and  $V_p$  should be appropriate for the  $\theta$ -type structure with only two kinds of values of transfer integrals  $t_c$  and  $t_p$ . However we approximate in the calculations also for the  $\theta_d$  and  $\alpha$ -type structures that only two kinds of the intersite Coulomb energy  $V_c$  and  $V_p$  exist since the deviation in the actual  $\theta_d$  and  $\alpha$ -(ET)<sub>2</sub>X, which both can be considered as structurally similar phases to the  $\theta$ -phase,<sup>41)</sup> is expected to be small.

### 2.3 Stripe-type charge ordered state

In the following sections the solutions with charge disproportionation of stripe-type are found to be relevant in some compounds, where the sites with more amount of charge are arranged in rows alternately. Three kinds of charge patterns, namely arrangements of holes, can be naturally considered as shown in Fig. 7, which we call the vertical stripes (a), the horizontal stripes (b) and the diagonal stripes (c), respectively. In Fig. 7, the schematic representation of the solutions with stripe-type CO which are found to be stabilized are shown. In Fig. 8(a) and (b) two examples for the CO state with vertical stripes for the  $\theta_d$ -type structure are displayed where the unit cells consist of 4 and 8 ETs ( $m = 4$  and  $m = 8$  in eq. 3), respectively, where the matrix elements of  $h_0$  and  $h_V$  for the former case of Fig. 8(a) are written as

$$\begin{aligned}
[h_0]_{ii} &= 0, \\
[h_0]_{12} &= \left([h_0]_{34}\right)^* = t_{c1}e^{ik_y/2} + t_{c2}e^{-ik_y/2}, \\
[h_0]_{13} &= 2t_{p2}e^{-ik_y/4}\cos(k_x/2), \\
[h_0]_{14} &= t_{p3}e^{i(k_x/2+k_y/4)} + t_{p1}e^{-i(k_x/2-k_y/4)}, \\
[h_0]_{23} &= t_{p1}e^{i(k_x/2+k_y/4)} + t_{p3}e^{-i(k_x/2-k_y/4)}, \\
[h_0]_{24} &= 2t_{p4}e^{-ik_y/4}\cos(k_x/2), \\
[h_0]_{ij} &= \left([h_0]_{ji}\right)^* \quad (i > j),
\end{aligned}$$

$$\begin{aligned}
[h_V]_{11} &= 2V_cn_2 + 2V_p(n_3 + n_4), \\
[h_V]_{22} &= 2V_cn_1 + 2V_p(n_3 + n_4), \\
[h_V]_{33} &= 2V_cn_4 + 2V_p(n_1 + n_2), \\
[h_V]_{44} &= 2V_cn_3 + 2V_p(n_1 + n_2), \\
[h_V]_{ij} &= 0 \quad (i \neq j).
\end{aligned}$$

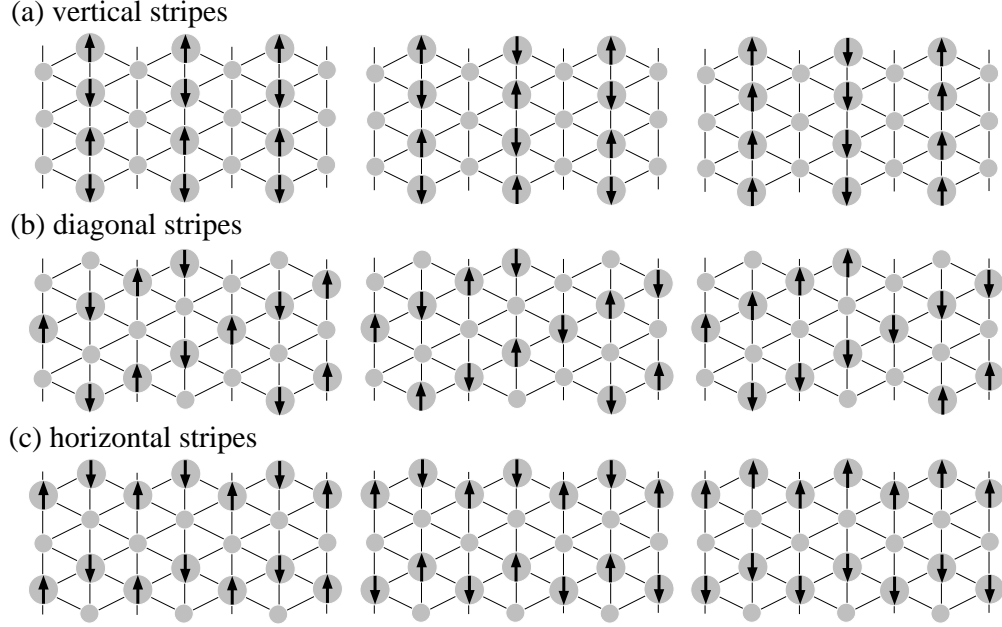


Fig. 7. Schematic representation of the spin moments and hole densities for the stripe-type CO solutions found to be stabilized. The diameters of the gray circles and the arrows represent the hole densities  $2 - \langle n_i \rangle$  and the spin moments, respectively.

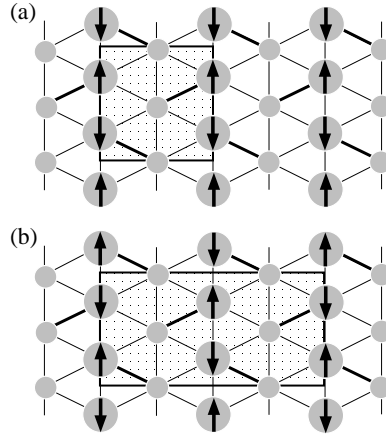


Fig. 8. The magnetic cell for two examples of vertical stripe-type CO solution for  $\theta_d$ -type structure. Thick lines represent the bonds with the largest transfer integral  $t_{p3}$ . The dotted areas, the larger gray circles and the arrows denote the unit cells, the sites with excess holes and the magnetic moments, respectively.

### §3. Results of Calculations

In self-consistent MF calculations, the 2D integrations are approximated by a sum of the mesh, where the analytical tetrahedron method is employed<sup>6,42)</sup> for  $30 \times 30$   $k$ -points per Broullian zone for the cell of four sites. In §3.1 - 3.3, the value of  $U$  is fixed at  $U = 0.7$  eV. The dependences on  $U$  are considered in §3.4.

#### 3.1 $\theta$ -type

The results for  $\theta$ -type structure reveal that stripe-type CO states have the lowest energy for relevant values of Coulomb energies, though the charge pattern depends on the parameters of the model, which are the transfer integrals  $t_c$  and  $t_p$  and the intersite Coulomb energies  $V_c$  and  $V_p$ . First we consider the case of  $t_c = 0.01$  eV and  $t_p = -0.1$  eV, the typical values for the series of  $\theta$ -(ET)<sub>2</sub>MM'(SCN)<sub>4</sub>,<sup>21)</sup> and the case of the isotropic intersite Coulomb interactions, i.e.  $V_c = V_p \equiv V$ . In Fig. 9, we show the  $V$ -dependence of the calculated relative energies for the solutions which are stable for  $0 \leq V/U \leq 1$  compared to the energy of the diagonal stripe solution schematically shown in an inset. The solutions which are not shown in the figure have higher energies. It can be seen that the vertical stripe solution with AF ordering both along and between these stripes (see inset of Fig. 9), has the lowest energy for  $V/U \leq (V/U)_{\text{cr1}} = 0.49$ , whereas for  $(V/U)_{\text{cr1}} \leq V/U \leq (V/U)_{\text{cr2}} = 0.51$ , the state with diagonal stripes does. For  $V/U \geq (V/U)_{\text{cr2}}$  a nonmagnetic insulating state is stable, which can be seen as a bipolaronic state with every fourth site being occupied by almost two holes, as schematically shown in an inset.

The value of  $(V/U)_{\text{cr1}}$  slightly varies when the values of transfer energies,  $t_c$  and  $t_p$ , are varied, though the qualitative behaviors are similar for  $t_c/|t_p| \lesssim 0.2$ , which is appropriate for  $\theta$ -(ET)<sub>2</sub>MM'(SCN)<sub>4</sub>.<sup>21)</sup> In Fig. 10 the phase diagram for the  $\theta$ -type structure is shown on the plane of  $V/U$  and  $t_c$ , with fixed values of  $U = 0.7$  eV and  $t_p = -0.1$  eV, excluding the bipolaronic state to see the competition between different stripe-type CO states. It can be seen that, concerning the charge pattern, the vertical stripes are preferred in the region of small  $V$  while the diagonal stripes are in the region of large  $V$  as an overall feature, though the spin configurations depend on the value of  $t_c$ .

Next we vary the value of  $V_p/V_c$  yet fixing  $U = 0.7$  eV,  $t_c = 0.01$  eV and  $t_p = -0.1$  eV. In Fig. 11, the  $V_p/V_c$ -dependence of the relative energy of the vertical stripe solution compared to the diagonal stripe solution for the case of  $V_c$  fixed at 0.25 eV is shown. Note that the other solutions have higher energies than these two solutions. As  $V_p/V_c$  is decreased, there exists a phase transition at  $(V_p/V_c)_{\text{cr}} = 0.95$  from the CO state with vertical stripes to the one with diagonal stripes. It is noteworthy that a very slight deviation from  $V_p/V_c = 1$ , where the state with vertical stripes is stable, makes the energy of the diagonal stripe solution lower, so the boundary between the vertical and diagonal stripes in Fig. 10, which is around  $V/U = 0.5$  for the isotropic case, is easily

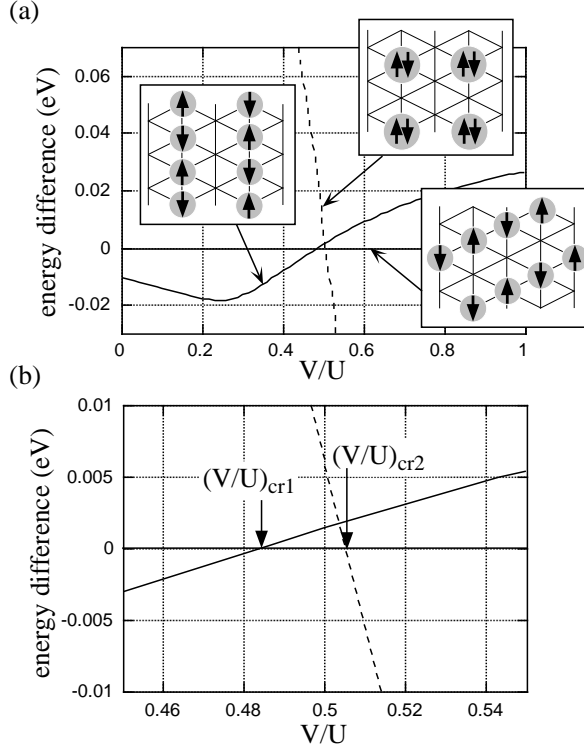


Fig. 9.  $V/U$  dependence of relative energy compared to the diagonal stripe solution which is schematically shown in an inset, for  $U = 0.7$  eV,  $t_c = 0.01$  eV and  $t_p = -0.1$  eV. The schematic representations of the charge pattern as well as the magnetic structure in these solutions are shown in insets. The enlargement of the critical region is shown in (b).

varied when  $V_p/V_c$  is varied.

### 3.2 $\theta_d$ -type

The calculations for the  $\theta_d$ -type structure show that several different types of charge patterns compete with each other when the values of intersite Coulomb energies are varied. In this subsection the transfer integrals are fixed to those in Fig. 1(c). In contrast to the  $\theta$ -type structure above, there exist three different charge patterns for horizontal stripe solutions which have different energies: the solutions with excess holes on sites 1 and 3 (stripes along  $t_{p3}$  and  $t_{p1}$ ), sites 1 and 4 (stripes along  $t_{p4}$ ), and sites 2 and 3 (stripes along  $t_{p2}$ ) as shown in Fig. 12(a)~(c), respectively. Among these states, the stripes along  $t_{p3}$  and  $t_{p1}$  have lower energies in the region of large  $V$  ( $V/U \gtrsim 0.5$ ), whereas for small  $V$  ( $V/U \lesssim 0.5$ ) the stripes along  $t_{p4}$  does. In Fig. 13, the ground state solutions are shown for the case of isotropic intersite Coulomb interactions,  $V_c = V_p \equiv V$ , as  $V/U$  is varied with  $U$  fixed at 0.7 eV. It can be seen there that when  $V$  is increased the charge pattern of

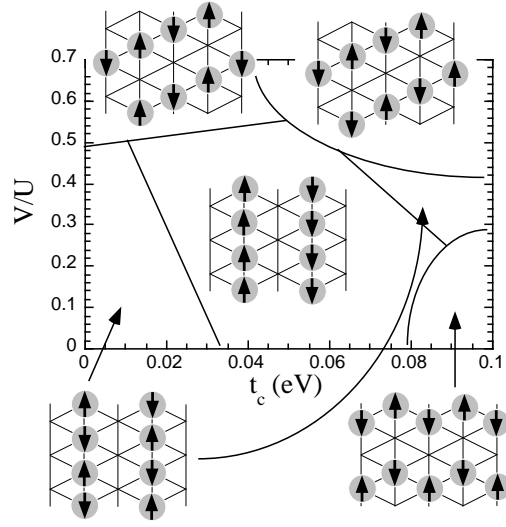


Fig. 10. The phase diagram for the  $\theta$ -type structure on the plane of  $V/U$  and  $t_c$ , for  $U = 0.7$  eV and  $t_p = -0.1$  eV, excluding the bipolaronic state.

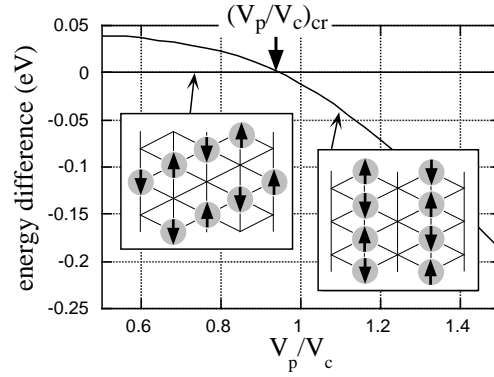


Fig. 11.  $V_p/V_c$  dependence of relative energy compared to the diagonal stripe solution which is schematically shown in the right inset, on the  $\theta$ -type structure for the fixed value of  $V_c = 0.25$  eV and  $U = 0.7$  eV.

the solution having the lowest energy varies from the vertical stripes to the bipolaronic state at  $V/U = (V/U)_{cr} = 0.50$ . In Fig. 14, the magnetic moment and the charge density on each site for the vertical stripe solution are shown as a function of  $V/U$ . As  $V$  is decreased, this stripe-type CO state continuously crosses over to the dimeric AF state, with almost same charge density on each site and AF ordering between dimers, i.e. pairs of molecules connected by the largest transfer

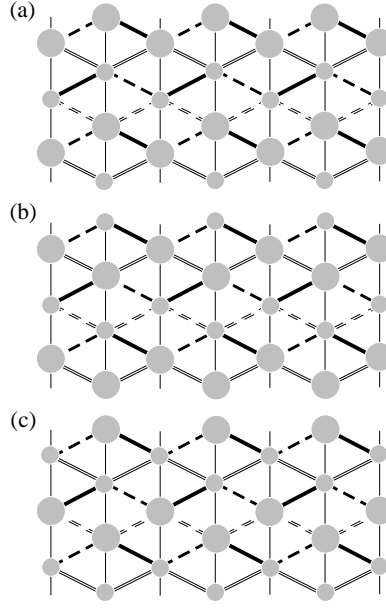


Fig. 12. Schematic representations of the charge pattern the three different horizontal stripes in  $\theta_d$ -type structure: stripes along  $t_{p3}$  and  $t_{p1}$  (a), those along  $t_{p4}$  (b) and those along  $t_{p2}$  (c). The thick dotted, double dotted, thick solid, double solid bonds represent the bonds with the transfer integral  $t_{p1}$ ,  $t_{p2}$ ,  $t_{p3}$ ,  $t_{p4}$ , respectively and the thin solid bonds are for  $t_{c1-2}$ .

energy  $t_{p3}$ , which is known to be stable for  $V = 0$ .<sup>35)</sup>

When  $V_p/V_c$  is varied, the solution which gives the lowest energy easily changes as in the case of  $\theta$ -phase. In Fig. 15, we show the variation of ground state solutions for the fixed value of  $V_c=0.25$  eV. For  $V_p/V_c \leq (V_p/V_c)_{\text{cr}} = 0.88$ , the state with diagonal stripes is stable, whereas there exists

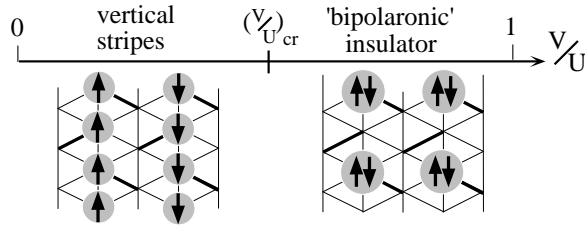


Fig. 13. The sequences of the solution which gives the lowest energy for  $\theta_d$ -type structure, as a function of  $V/U$  ( $U = 0.7$  eV). The thick bonds represent the bonds with the largest transfer energy  $t_{p3}$ , as in Fig. 8.

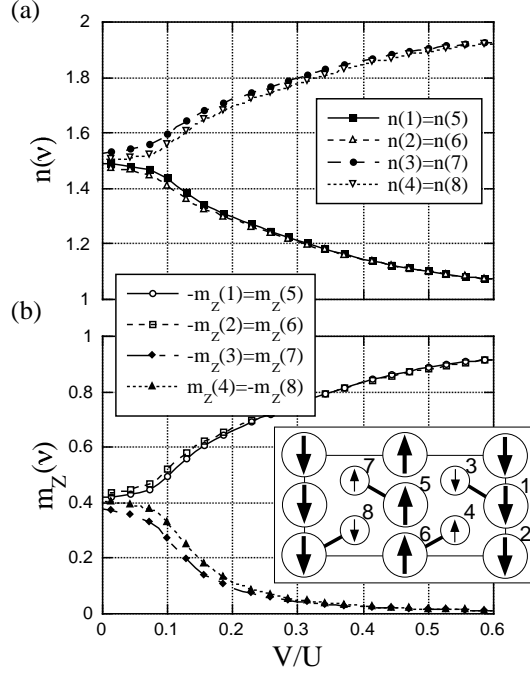


Fig. 14.  $V/U$  dependence of the charge densities (a) and magnetic moments (b) on each site for the state with vertical stripes which gives the lowest energy in the region of small  $V$  for the  $\theta_d$ -type structure. Inset shows the indices for sites and schematically the charge pattern and the magnetic structure in this vertical stripe solution, where the thick bonds describe the bonds with largest transfer energy  $t_{p3}$ , the sites with large (small) arrows and those with large (small) diameters represent the sites with large (small) hole density and those with large (small) magnetic moment while the direction of the arrows shows the direction of spins.

another solution with almost same energy: the horizontal stripes along  $t_{p4}$ , as shown in Fig. 15. For  $V_p/V_c \geq (V_p/V_c)_{cr}$  the vertical stripe solution has the lowest energy, as in the case of  $\theta$ -phase.

### 3.3 $\alpha I_3$ -type and $\alpha MHg$ -type

The calculations for the  $\alpha$ -type structures show that the diagonal stripe solutions have rather high energies compared to the other stripe-type CO states, which is in contrast to the above cases for the  $\theta$  and  $\theta_d$ -type structures. In this subsection the transfer integrals are fixed to those in Fig. 1(a). Due to the lower symmetry than the  $\theta$ -type structure, as in the  $\theta_d$ -phase, concerning the vertical and the horizontal stripes each has two solution with different charge patterns having different energies: as for the vertical stripes those along stack I and those along stack II, and for the horizontal stripes those along  $t_{p2}$  and  $t_{p3}$  and those along  $t_{p1}$  and  $t_{p4}$ , which are shown in Fig. 16.

In the upper part of Fig. 17, the sequences of ground state solutions for the  $\alpha I_3$ -type structure



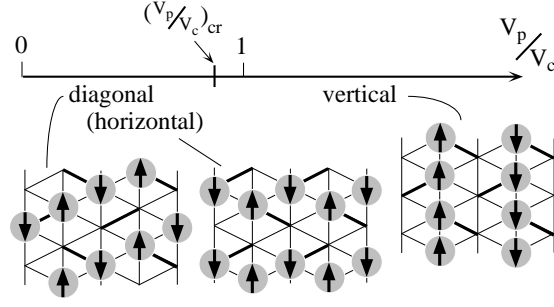


Fig. 15. The  $V_p/V_c$ -dependence of the solution which gives the lowest energy for  $\theta_d$ -type structure, for the case of  $V_c = 0.25$  eV and  $U = 0.7$  eV.

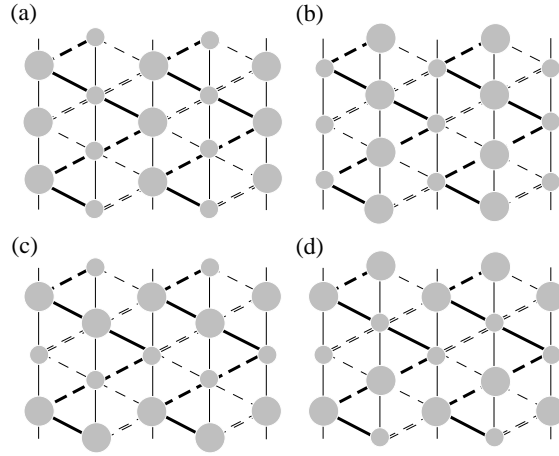


Fig. 16. Schematic representations of the charge patterns for the different horizontal stripes and vertical stripes in the  $\alpha$ -type structure: vertical stripes along stack I (a), those along stack II (b), horizontal stripes along  $t_{p2}$  and  $t_{p3}$  (c) and those along  $t_{p1}$  and  $t_{p4}$  (d). The thick dotted, thick solid, double dotted, thin dotted bonds represent the bonds with transfer integrals  $t_{p1}$ ,  $t_{p2}$ ,  $t_{p3}$ ,  $t_{p4}$ , respectively and the thin solid bonds are for  $t_{c1\sim3}$ .

for the case of isotropic intersite Coulomb interactions,  $V_c = V_p \equiv V$ , are shown. As  $V$  is increased, the state which is stable varies from the one with vertical stripes on stack II, to the one with another vertical stripes on stack I at  $V/U = (V/U)_{cr1} = 0.27$ . KF concluded that the latter state was the ground state of  $\alpha$ -(ET)<sub>2</sub>I<sub>3</sub> for  $V = 0$  under the assumption that the magnetic cell consists of four molecules which is identical to the structural unit cell,<sup>3)</sup> but the considerations of larger cells in the present calculation indicate that at  $V = 0$  the vertical stripe solution with the other

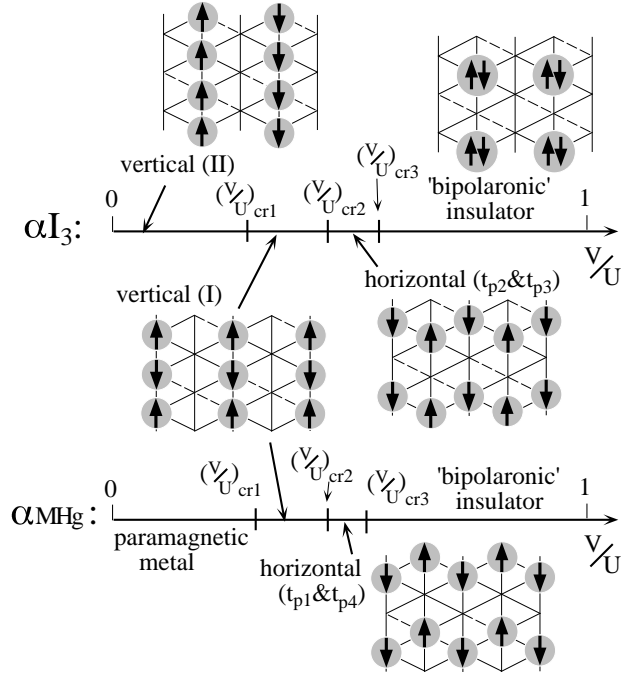


Fig. 17. The sequences of the solution which gives the lowest energy for  $\alpha$ -type structures, as a function of  $V/U$  ( $U = 0.7$  eV). The dotted bonds represent the transfer integral  $t_{p4}$ . The distinction between different stripes among the vertical stripes on stack I or II and among the horizontal stripes along  $t_{p2}$  and  $t_{p3}$ , and  $t_{p1}$  and  $t_{p4}$  are also described here.

charge pattern, i.e. the stripes on stack II, has lower energy. As  $V$  is increased further, a phase of horizontal stripes along  $t_{p2}$  and  $t_{p3}$  appears at  $V/U = (V/U)_{cr2} = 0.43$  and a bipolaronic state takes place above  $V/U = (V/U)_{cr3} = 0.50$ .

In Fig. 18, we show the  $V_p/V_c$ -dependence of the ground state solutions for the case of fixed value of  $V_c=0.25$  eV. As in the calculations for the  $\theta$  and  $\theta_d$ -type structures, the solution which has the lowest energy easily changes from that for the case of isotropic inter-site Coulomb interactions, when the value of  $V_p/V_c$  is deviated from 1. The solution with horizontal stripes along  $t_{p2}$  and  $t_{p3}$  has the lowest energy for  $V_p/V_c \leq (V_p/V_c)_{cr} = 0.96$ , whereas the one with vertical stripes on stack I is stable for  $V_p/V_c \geq (V_p/V_c)_{cr}$ .

In the work of KF, Hartree-Fock calculations for  $U = 0.7$  on the  $\alpha$ MHg-type structure suggest a paramagnetic metallic (PM) ground state.<sup>5)</sup> By including  $V_{i,j}$  some CO phases appear, as can be seen in the lower part of Fig. 17 where the ground state solutions for the case of isotropic inter-site Coulomb interactions,  $V_p = V_c \equiv V$ , are shown. The ground state changes from the PM phase, as  $V$  is increased, to a CO phase with the vertical stripes on stack I at  $V/U = (V/U)_{cr1} = 0.32$ . As

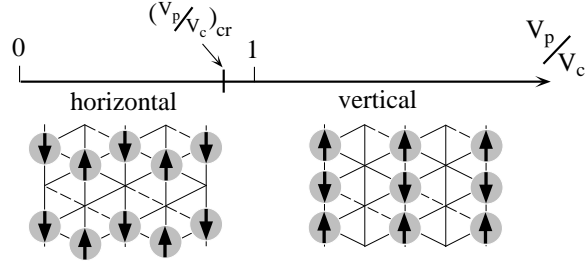


Fig. 18.  $V_p/V_c$  dependence of the solution which gives the lowest energy for the  $\alpha I_3$ -type structure with  $V_c = 0.25$  eV and  $U = 0.7$  eV.

$V$  is increased further a phase transition is present at  $V/U = (V/U)_{cr2} = 0.46$  to a phase of the horizontal stripes along  $t_{p1}$  and  $t_{p4}$ , and above  $V/U = (V/U)_{cr3} = 0.54$  the bipolaronic state has the lowest energy. As can be seen by comparing the upper and lower parts of Fig. 17, the sequences of ground states for the  $\alpha M Hg$  and  $\alpha I_3$ -type structures are qualitatively similar for  $V/U \geq (V/U)_{cr1}$ , although the charge pattern for the horizontal stripes stable for  $(V/U)_{cr2} \leq V/U \leq (V/U)_{cr3}$  are different to each other. In Fig. 19, the charge density, the magnetic moment on each site, and the band gap for the solution with vertical stripes on stack I for the  $\alpha I_3$  and  $\alpha M Hg$ -type structures as a function of  $V/U$  is plotted which are stable for  $(V/U)_{cr1} \leq V/U \leq (V/U)_{cr2}$ . The notation of ‘band gap’ is the same as in the work of KF,<sup>6)</sup> which is the value of the bottom of the 1st band minus the top of the 2nd band for the actual case with the unit cell of 4 sites ( $m = 4$  in eq. 3). It can be seen that both solutions show qualitatively similar features though the CO state for the  $\alpha M Hg$ -type structure has relatively small values of band gap compared to those for the  $\alpha I_3$ -type structure.

### 3.4 Simplified model for $(ET)_2X$

As have been seen in §3.1 - 3.3 the CO states are more stabilized by the intersite Coulomb interactions  $V_{ij}$ . In contrast, although the presence of relevant values of  $V_{ij}$  can be expected in the actual  $\kappa$ -type compounds which have large dimerization, the dimeric AF state in their insulating phase is confirmed experimentally to be stable,<sup>8)</sup> consistent with the MF calculations by KF without  $V_{i,j}$ . Here to investigate the competition between this dimeric AF state and the CO states, and to get insight into a unified view of the electronic properties of  $(ET)_2X$ , calculations are performed on the model in Fig. 3(b) by varying  $t_{p1}$  or  $t_{p4}$ .

Only the case for the isotropic intersite Coulomb interaction  $V$  is considered and the values of  $t_c$  and  $t_p$  are fixed at 0.01 eV and 0.1 eV, respectively. We just take into account a vertical stripe CO state described in the inset of Fig. 20. Other stripe-type solutions may have lower energy in some

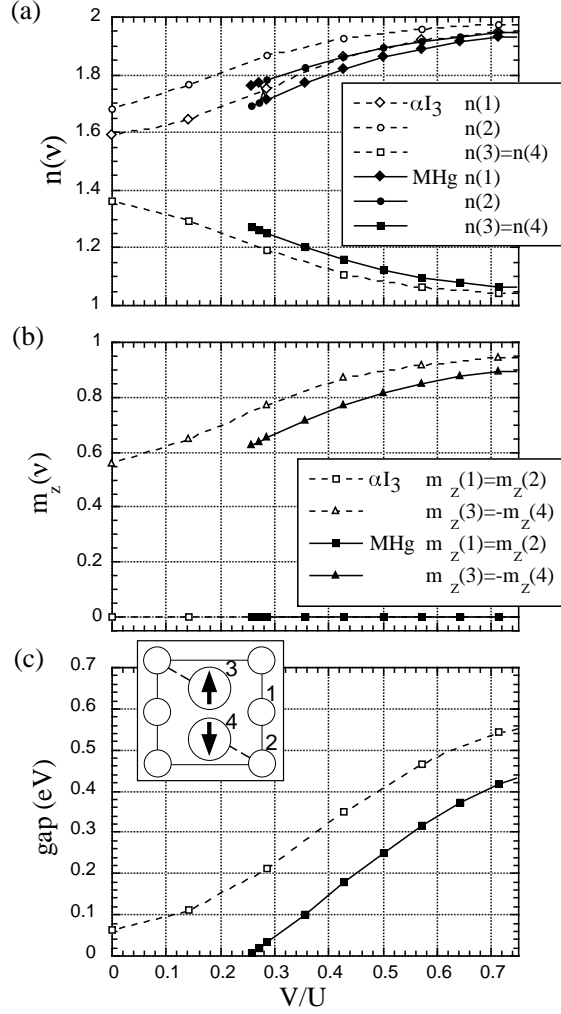


Fig. 19.  $V/U$  dependence of the charge density (a), the magnetic moment (b) and the band gap (c) on each site for the solutions with vertical stripes on stack I for  $\alpha MHg$ -type and  $\alpha I_3$ -type structures for  $U = 0.7$  eV.

parameter region but the qualitative features on the competition between the stripe-type CO state and other states, whose investigation is our aim, should be made. Note that we know from §3.1 that this state is stable in the case of  $t_{p1} = t_{p4} = t_p$ , identical to the  $\theta$ -type structure with  $t_p = 0.1$  eV and  $t_c = 0.01$  eV, and  $V/U \leq 0.49$ .

First we fix  $t_{p4} = t_p$ , and vary the Coulomb interactions  $U$ ,  $V$  and the degree of dimerization  $t_{p1}$ . The phase diagram for  $V = 0$  on the plane of  $U$  and  $t_{p1}$  is shown in Fig. 20(a), which is similar to the corresponding phase diagram for the  $\kappa$ -type structure obtained by KF,<sup>4,6)</sup> again suggesting that this simplified model can be considered as an effective model for the family of  $(ET)_2X$ . In the large  $U$  region, the AF insulating state emerges which is the dimeric AF state, and becomes

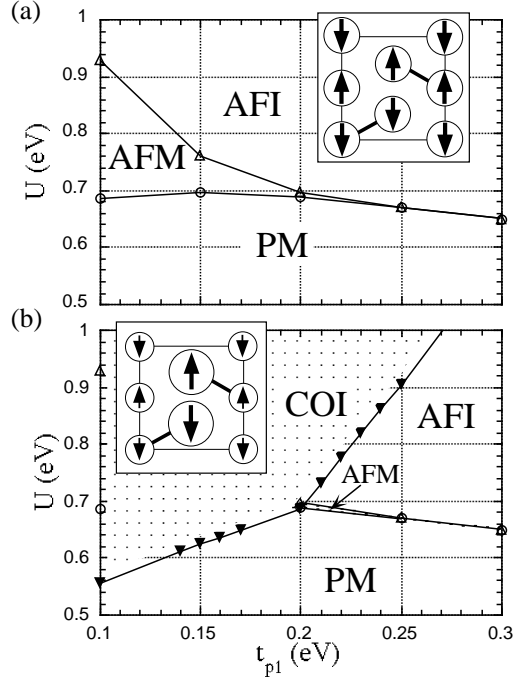


Fig. 20. Phase diagrams of the model structure in Fig. 3 on the plane of  $U$  and  $t_{p1}$ , in the case of  $t_{p4} = t_p = 0.1$  eV for  $V = 0$  (a) and for  $V/U = 0.25$  (b). COI, AFI, AFM and PM denote the charge ordered insulating, antiferromagnetic insulating, antiferromagnetic metallic and paramagnetic metallic phases, respectively.

more stabilized as  $t_{p1}$  is increased. When  $V$  is turned on, there appears the CO phase. The phase diagrams on the plane of  $U$  and  $V/U$  for  $t_{p1} = 0.30$  eV and  $t_{p1} = 0.15$  eV are shown in Fig. 21(a) and (b), respectively. It can be seen that the stripe-type CO phase is stabilized when  $V$  exceeds some critical value, *e.g.* 0.150 eV for  $t_{p1} = 0.15$  eV and  $U = 0.7$ . The bipolaronic state has the lowest energy when  $V$  is larger than approximately  $U/2$ , similar to the results in §3.1-3.3. If we consider the stripe-type CO state with 1 hole on each site along the stripes and the bipolaronic state with 2 holes on every 4 sites which will be stabilized in the limit of  $U, V \rightarrow \infty$ , the energy loss in the Coulomb interactions in the stripe-type CO state and the bipolaronic CO state will be  $2V$  and  $U$  per unit cell of four sites, respectively, so the critical value of  $V \simeq U/2$  can be easily understood. As can be seen in Fig. 22, where the charge density and the magnitude of spin density at each site together with the band gap are displayed for  $t_{p1} = 0.15$  eV, the phase transition from the AF insulating phase to the CO insulating phase at  $V_{cr1}$  is a second-order transition for  $U = 0.8$  eV, whereas the one from the metallic phases to the CO insulating phase is a first-order one for  $U = 0.7$  eV and 0.6 eV. The stripe-type CO phase which has appeared by the inclusion of  $V$  can be described on the plane of  $U$  and  $t_{p1}$  as in Fig. 20(b), where the phase diagram in the case of fixed

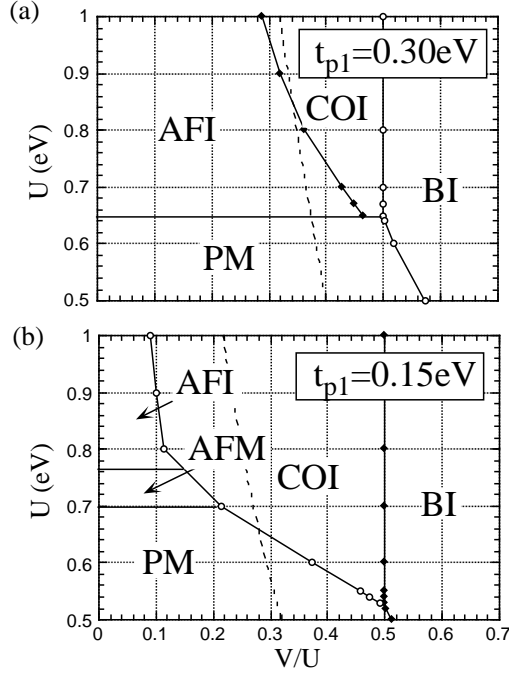


Fig. 21. Phase diagrams of the model structure in Fig. 3 in the plane of  $U$  and  $V/U$ , for the case of  $t_{p1} = 0.30$  eV (a) and  $t_{p1} = 0.15$  eV (b), where  $t_c$  and  $t_{p4} = t_p$  are fixed at 0.01 eV and 0.1 eV, respectively. The notations for COI, AFI, AFM and PM are the same as in Fig. 20, and BI denotes the bipolaronic insulating phase. The dotted lines show the relation  $2t_{p1} + U/2(1 - \sqrt{1 + (4t_{p1}/U)^2}) = V$ , which is discussed in §4.4

ratio of  $V/U = 0.25$  is shown. It can be seen that for  $t_{p1} \lesssim 0.2$  eV, where the dimerization is small, the dimeric AF phase is overwhelmed by the stripe-type CO phase, whereas when the dimerization is large enough as  $t_{p1} \gtrsim 0.2$  eV this dimeric AF phase survives.

Next we fix  $t_{p1} = t_p$ , and vary  $t_{p4}$ , so that the band overlap can be controlled, corresponding to the case of  $\alpha$ -type compounds. The phase diagram for  $V = 0$  on the plane of  $U$  and  $t_{p4}$  is shown in Fig. 23, where the general features are similar to the Hartree-Fock phase diagram for the  $\alpha$ -type structure obtained by KF,<sup>3,6)</sup> as expected. The decrease in the value of  $t_{p4}$  leads to the stabilization of the CO state, where the charge pattern and the spin configuration are schematically shown in the inset of Fig. 23(b). By the inclusion of  $V$  the stripe-type CO phase is stabilized further. Phase diagrams on the plane of  $U$  and  $V/U$  for the case of  $t_{p4} = 0.03$  eV and 0.09 eV are shown in Fig. 24(a) and (b), respectively. It can be seen that the stripe-type CO phase is stabilized in a wide range of parameters, while the bipolaronic state again has lower energy for  $V \gtrsim U/2$ . In Fig. 25, the charge density and the magnitude of spin density at each site together with the band gap are shown for the choice of  $t_{p4} = 0.09$  eV. Here the phase transition as a function of  $V$  is of second-

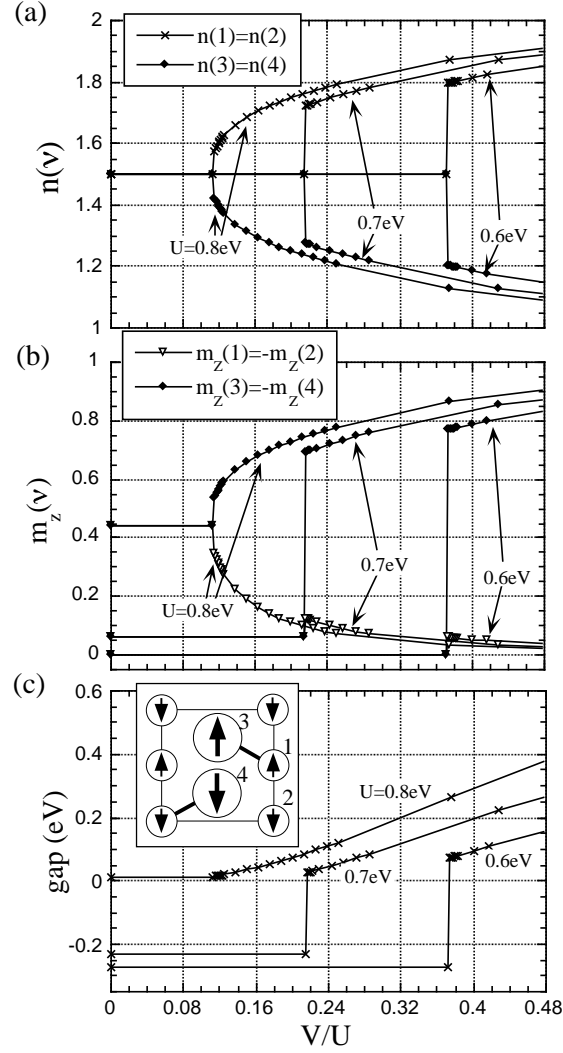


Fig. 22.  $V$  dependence of the charge density (a), the magnetic moment (b) on each site, and the band gap (c), for the case of  $t_{p1} = 0.15$  eV,  $t_{p4} = t_p = 0.1$  eV,  $t_c = 0.01$  eV and  $U = 0.8, 0.7, 0.6$  eV.

order-type when it is from the CO metallic phase to the CO insulating phase for  $U = 0.8$  eV and 0.7 eV, and the one from the PM phase to the CO insulating phase is a first-order one for  $U = 0.6$  eV. The phase diagram on the plane of  $U$  and  $t_{p4}$  for the fixed ratio of  $V/U = 0.25$  is shown in Fig. 23(b), where the CO phase extends compared to the case of  $V = 0$ , especially in the region of large  $t_{p4}$ .

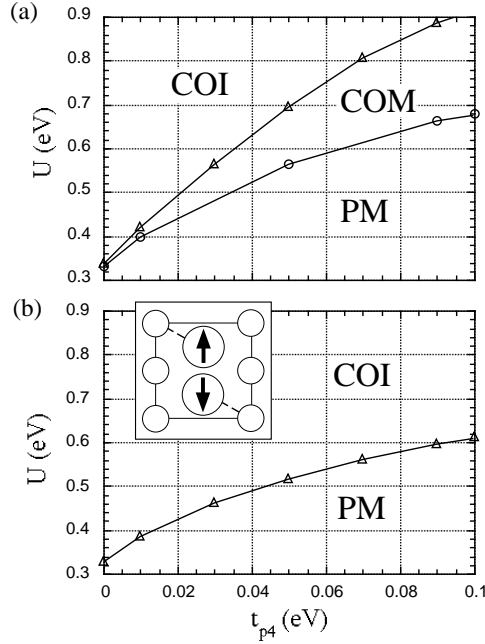


Fig. 23. Phase diagrams of the model structure in Fig. 3 on the plane of  $U$  and  $t_{p4}$ , in the case of  $t_{p1} = t_p = 0.1$  eV for  $V = 0$  (a) and for  $V/U = 0.25$  (b). COI, COM and PM denote the charge ordered insulating, charge ordered metallic and paramagnetic metallic phases, respectively.

#### §4. Discussions

In the previous section, it was seen that stripe-type CO states are stabilized in general, while the actual spatial pattern of charge density sensitively depends on the parameters of models, i.e. the anisotropy of the transfer integrals and the values of intersite Coulomb energies. In order to find out whether these CO states are realized in the actual compounds, and, if they are, which type of stripes are realized, the comparison between our calculation and the properties observed in experiments will be pursued in the following, since the value of the intersite Coulomb energies  $V_{i,j}$  as well as its degree of anisotropy  $V_p/V_c$  is difficult to determine by theories above. In pursuing this, however, we adopt from the studies<sup>36)</sup> mentioned in §1 the ratio of the neighboring Coulomb energies  $V_c, V_p$  to the on-site one  $U$  to be  $V_c/U, V_p/U \simeq 0.2 - 0.5$  and  $V_p/V_c$  to be about 1.

To reconcile the results of the MF calculations showing ordering of spins to the observed properties where magnetically ordered ground states are frequently destroyed by quantum fluctuation which is neglected in our approximation, the effects of this quantum fluctuation is incorporated by mapping the stripe-type CO states to the  $S = 1/2$  Heisenberg Hamiltonians where these spins are interacting by the superexchange interactions  $J_{i,j}$  deduced from the transfer integrals in Fig. 1.<sup>44)</sup> Although



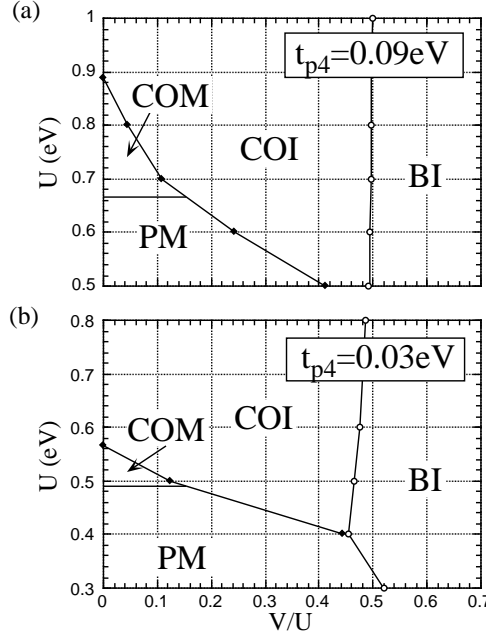


Fig. 24. Phase diagrams of the model structure in Fig. 3 in the plane of  $U$  and  $V/U$ , for the case of  $t_{p4} = 0.03$  eV (a) and  $t_{p4} = 0.09$  eV (b), where  $t_c$  and  $t_{p1} = t_p$  eV are fixed at 0.01 eV and 0.1 eV, respectively. The abbreviations for COI, COM and PM are same as in Fig. 23, and BI stands for the bipolaronic insulating phase.

the estimation of the values of  $J_{i,j}$  along the stripes will be done in the following by using the relation  $J_{i,j} \sim 4t_{i,j}^2/U$  with  $U = 0.7$  eV, we note that the definite values should not be taken seriously, but only the relative values should, since there is ambiguity on both the value of  $U$  and the transfer integrals based on the simple semi-empirical extended Hückel method. However, as a general trend, the exchange couplings get reduced from these values of  $J_{i,j} \sim 4t_{i,j}^2/U$  in the charge ordered state with intermediate charge disproportionation,<sup>43)</sup> thus it is natural that the exchange couplings deduced from experiments are smaller than those naively estimated from this relation.

#### 4.1 $\theta$ -phase

The general features in the phase diagram in Fig. 10 can be understood as follows. In the region of small  $V$ , the holes tend to form stripes along the direction with smaller transfer energy  $t_c$ , i.e. the vertical stripes, so that they can gain kinetic energy along the bonds with  $t_p$ . On the other hand, the holes are expected to have much localized character in the region of large  $V$ , then to gain exchange energy along the stripes they choose the stripes with larger exchange energy  $J_p \sim 4t_p^2/U$ , i.e. the diagonal stripes along  $t_p$ .

When  $t_c = 0$ , the topology of our model is identical to that of the 2D square lattice model with

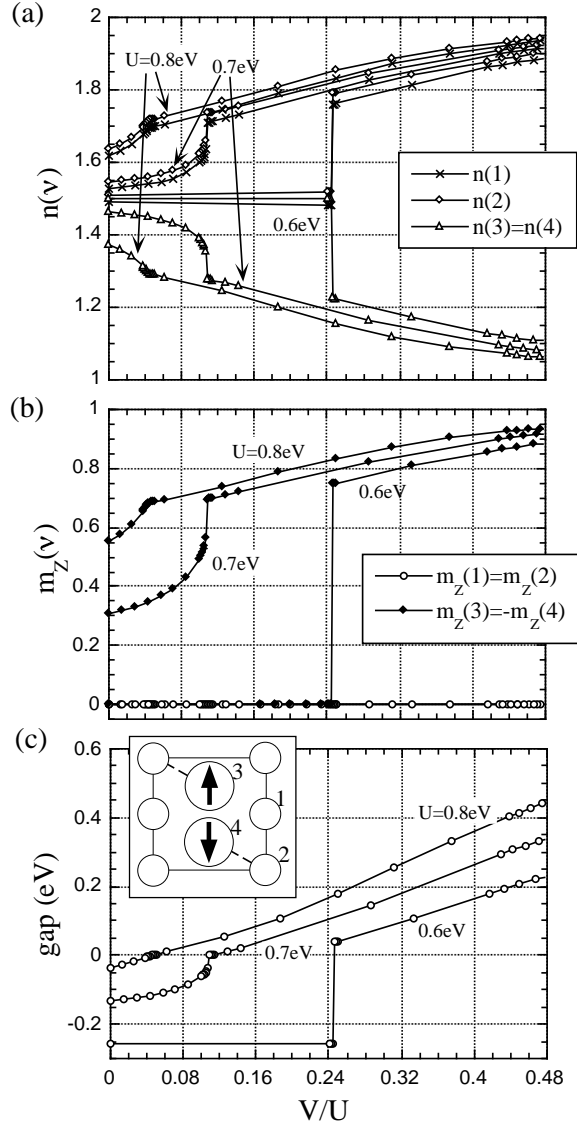


Fig. 25.  $V$  dependence of the charge density (a), the magnetic moment (b) on each site, and the band gap (c), for  $t_c = 0.01 \text{ eV}$ ,  $t_{p1} = t_p = 0.1 \text{ eV}$ ,  $t_{p4} = 0.09 \text{ eV}$  and  $U = 0.8, 0.7, 0.6 \text{ eV}$ .

nearest neighbor transfer integral  $t = t_p$ . The results above for small  $V$  that the vertical stripes along the smaller transfer integral  $t = t_c$  are stable, is similar to the results in theoretical studies on the Hubbard model on such 2D square lattice, where the stability of stripes along the bonds for  $U/|t| \lesssim 4$  and those along the diagonal direction of the bonds for  $U/|t| \gtrsim 4$  has been indicated,<sup>45)</sup> since our calculations were performed for the value of  $U/|t_p| = 7$ , which correspond to the latter case, and the vertical stripes in our notation are along the diagonal direction of the bonds with the

larger transfer integral  $t_p$ , although the filling of  $n = 1/4$  in our calculations is different from the above studies for  $n = 1/2 - x$  with  $x \sim 0$ .

From the MF calculations, the candidates for the ground state of the insulating phase in actual  $\theta$ -type compounds are the CO states with vertical stripes and those with diagonal stripes. The bipolaronic state is not likely realized since the ground state in these compounds are magnetic, as disclosed by the magnetic susceptibility measurement.<sup>21)</sup> When the CO states with the vertical stripes and the diagonal stripes are mapped to 1D  $S = 1/2$  Heisenberg models, the AF couplings between the localized spins can be deduced to be the order of  $J_c \sim 4t_c^2/U = 10$  K and  $J_p \sim 4t_p^2/U = 500$  K, respectively. The magnetic susceptibilities measured in experiments for  $\theta$ -(ET)<sub>2</sub>RbZn(SCN)<sub>4</sub> with rapid cooling condition and for  $\theta$ -(ET)<sub>2</sub>CsZn(SCN)<sub>4</sub> show Curie-like behaviors,<sup>21, 25)</sup> suggesting small values of exchange coupling between localized spins, which may indicate the vertical stripes, also inferred from the reflectivity measurement on  $\theta$ -(ET)<sub>2</sub>RbZn(SCN)<sub>4</sub> and  $\theta$ -(ET)<sub>2</sub>RbCo(SCN)<sub>4</sub> with rapid cooling condition.<sup>46)</sup> On the other hand the NMR data on  $\theta$ -(ET)<sub>2</sub>RbZn(SCN)<sub>4</sub> with rapid cooling condition suggest that the charge density on molecules becomes continuously distributed by decreasing temperature,<sup>47)</sup> as in the case of the incommensurate CDW state. This is in contrast with situation in the  $\theta_d$ -phase discussed in the next subsection and apparently inconsistent with our stripe-type CO state suggesting only two kinds of molecules with different charge densities. However, since there are two degenerate CO states with vertical stripes in the  $\theta$ -type structure, the dynamical motions of stripes may exist down to low temperature, making difficult to detect the stripe-type CO state by NMR experiments. This charge fluctuation may also be the origin for the apparently small couplings between spins, inferred from the magnetic susceptibility measurements. The interchain couplings between the spin on these vertical stripes show frustration due to the structure (see Fig. 1(b)), which is consistent with the absence of AF long range order down to 2 K.<sup>25)</sup>

Nevertheless, a recent X-ray study on another member of this family,  $\theta$ -(ET)<sub>2</sub>CsCo(SCN)<sub>4</sub>,<sup>48)</sup> shows a diffusive spot at  $(0, 0, 1/2)$  below 20 K which is proposed to be due to the existence of short range CO along the  $c$ -axis with period of 2 ET molecules, which is the case of the horizontal stripes or the diagonal stripes. The discrepancy between this fact and the conclusion above of the existence of CO state with vertical stripes in  $\theta$ -type compounds based on experimental results on members with  $MM' = \text{RbZn, RbCo and CsZn}$ , may be due to the tendency toward structural instability in  $\theta$ -(ET)<sub>2</sub>CsCo(SCN)<sub>4</sub>, i.e. toward the  $\theta_d$ -type structure as in  $\theta$ -(ET)<sub>2</sub>RbZn(SCN)<sub>4</sub>, and the fact that X-ray experiments are more sensitive to the lattice distortion than to the charge disproportionation. This possibility has also been pointed out by T. Mori *et al* from thermoelectric power measurements.<sup>49)</sup> Another possibility is that the charge pattern of the stripes is different between the members of  $\theta$ -(ET)<sub>2</sub> $MM'$ (SCN)<sub>4</sub> with  $MM' = \text{RbZn, RbCo and CsZn}$ , and the salt with  $MM' = \text{CsCo}$ , although their ET layers are isostructural.

## 4.2 $\theta_d$ -phase

The stability of the CO state with horizontal stripes in our MF calculations for the  $\theta_d$ -type structure compared to the results for the  $\theta$ -type one where the horizontal stripe solutions have rather high energies, may be related to the fact that the PM state in the  $\theta_d$ -type structure, which is the ground state for small  $U$  and  $V$ , shows slight charge disproportionation with pattern of charge density similar to that of the horizontal stripe-type CO state described in Fig. 15.

There are several candidates for the CO state realized in the insulating phase of the actual compounds in  $\theta_d$ -phase based on our calculations. Among them it can be deduced that the vertical stripes are not realized in  $\theta_d$ -(ET)<sub>2</sub>RbZn(SCN)<sub>4</sub> since the temperature dependence of the magnetic susceptibility data for 15 K  $\lesssim T \leq T_{\text{str}} = 195$  K suggest a larger exchange coupling,  $J \sim 160$  K,<sup>21,50)</sup> than those inferred from the vertical stripes,  $J_{c1} \sim 4t_{c1}^2/U = 50$  K and  $J_{c2} \sim 4t_{c2}^2/U = 100$  K. From this experimental fact, it is clear that the bipolaronic state with no spins again can be excluded. The remaining candidates are the diagonal stripes and the horizontal stripes along  $t_{p4}$  as shown in Fig. 15. The CO state with diagonal stripes leads to Heisenberg chains of four kinds of couplings,  $J_{p1} - J_{p4}$ , which may have a spin gap at the ground state but inconsistent with the Bonner-Fisher behavior in the magnetic susceptibility data for 15 K  $\lesssim T \leq T_{\text{str}}$  mentioned above. The CO state with horizontal stripes along  $t_{p4}$ , which we consider to be most likely, is mapped to Heisenberg  $S = 1/2$  chains with a uniform exchange coupling  $J_{p4} \sim 4t_{p4}^2/U = 450$  K, which is consistent with this Bonner-Fisher behavior and also with a reflectivity measurement suggesting the existence of the horizontal stripes in this compound.<sup>46)</sup> If this charge pattern is realized, the spin gap behavior seen in experiments<sup>21,25,19)</sup> is probably due to the spin-Peierls transition along these chains. Note that the lattice distortion expected in the spin-Peierls transition for this case does not produce superlattices since the unit cell along the  $b$ -direction initially contains two ET molecules in the  $\theta_d$ -type structure. The reflectivity data on the  $\theta_d$ -phase of another member (ET)<sub>2</sub>RbCo(SCN)<sub>4</sub> with slowly cooling condition also suggest the horizontal stripes,<sup>46)</sup> thus it may be concluded that the  $\theta_d$ -type structure in general favors the horizontal stripes.

Finally we comment on the recent experiment by Miyagawa *et al*<sup>19)</sup> who have performed a careful <sup>13</sup>C-NMR measurement on  $\theta$ -(ET)<sub>2</sub>RbZn(SCN)<sub>4</sub> on the condition of slowly cooling, where the  $\theta_d$ -type structure is observed below  $T_{\text{str}}$ . Their conclusion of the existence of two kinds of ETs with equal population in the ground state is consistent with our conclusion that the horizontal stripes along  $t_{p4}$  are realized in this compound, since in this horizontal stripe solution the charge density  $n(\nu)$  on the crystallographically equivalent molecules ‘1’ and ‘4’, and ‘2’ and ‘3’ (see Fig. 1) are respectively equal, i.e.  $n(1) = n(4)$  and  $n(2) = n(3)$ , which is not the case in other candidates mentioned above showing more than four kinds of ETs with different charge densities (*e.g.* see Fig. 14). Their data showing a broad line and a sharp Pake doublet, ascribed to the molecules with rich and less charge density, respectively, at  $15 \text{ K} \leq T \lesssim T_{\text{str}}$  seem to suggest that the charge

fluctuation along the stripes are large while in the transverse direction the stripes are ‘pinned’, which may explain why the resistivity shows a sudden increase at  $T_{\text{str}}$  as lowering the temperature. At around the temperature where the broad line turns into a clear Pake doublet ( $\sim 10$  K) the magnetic susceptibility also shows the drop. If it is the spin-Peierls transition temperature, this result implies that the lattice distortion along the stripes rapidly suppress the charge fluctuation.

Here we have not discussed the physical origin of the structural phase transition at  $T = T_{\text{str}}$ , since the lattice degree of freedom was not included in our calculations. However, it is possible that the emergence of the CO state with horizontal stripes and the lattice distortion from  $\theta$ -type to  $\theta_d$ -type structure occur cooperatively, as been discussed in La based high- $T_c$  Cuprates, in the context of the relation between the stripe formation and the low temperature tetragonal lattice distortion.<sup>51)</sup>

#### 4.3 $\alpha$ -(ET)<sub>2</sub>I<sub>3</sub> and $\alpha$ -(ET)<sub>2</sub>MHg(SCN)<sub>4</sub>

The difference between results for the  $\alpha$ I<sub>3</sub> and  $\alpha$ MHg-type structures concerning the charge patterns in the stable horizontal stripe solution for  $(V/U)_{\text{cr}2} \leq V/U \leq (V/U)_{\text{cr}3}$  can be understood when the exchange energies along the stripes,  $J_{p1-p4} \sim 4t_{p1-p4}^2/U$ , are considered. The two horizontal stripes are those along  $t_{p2}$  and  $t_{p3}$  and those along  $t_{p1}$  and  $t_{p4}$ , lead to gains in exchange energies of  $J_{p2} \sim 4t_{p2}^2/U$  and  $J_{p3} \sim 4t_{p3}^2/U$ , and  $J_{p1} \sim 4t_{p1}^2/U$  and  $J_{p4} \sim 4t_{p4}^2/U$ , respectively. In the  $\alpha$ I<sub>3</sub>-type structure, the value of  $|t_{p4}|$  is quite small compared to  $|t_{p1-3}|$  resulting in  $J_{p1} + J_{p4} < J_{p2} + J_{p3}$ , thus the calculations showing the stability of the horizontal stripes along  $t_{p2}$  and  $t_{p3}$  with larger gain of exchange energies can be explained. On the other hand, in the  $\alpha$ MHg-type structure the values of  $J_{p1-p4}$  are similar but  $J_{p1} + J_{p4}$  is slightly larger than  $J_{p2} + J_{p3}$ , which is consistent with the calculations indicating the horizontal stripes along  $t_{p1}$  and  $t_{p4}$  and the calculated energies of the two CO states with horizontal stripes are close to each other.

An explanation we propose here for the observed properties in  $\alpha$ -(ET)<sub>2</sub>I<sub>3</sub> is that the stripe-type CO state is realized below  $T_{\text{MI}}$ , though the charge pattern is different from the one proposed by KF which is the vertical stripes on stack I.<sup>3)</sup> The candidates for its ground state based on our MF calculations are two kinds of vertical stripe states, a horizontal stripe state and the bipolaronic state, as shown in Fig. 17. The bipolaronic state may explain the experimental results since a nonmagnetic behavior is seen in the susceptibility measurements, though the required value of  $V/U \gtrsim (V/U)_{\text{cr}3} = 0.54$  in our calculation is rather large. The estimations of exchange coupling along the stripes for the stripe-type CO states lead to uniform  $J_{c1} \sim 4t_{c1}^2/U = 50$  K in the case of the vertical stripes along stack II, and to alternating  $J_{c2} \sim 4t_{c2}^2/U = 140$  K and  $J_{c3} \sim 4t_{c3}^2/U = 30$  K in the case of those along stack I. The CO state we propose here to be realized in  $\alpha$ -(ET)<sub>2</sub>I<sub>3</sub> is the horizontal stripes along  $t_{p2}$  and  $t_{p3}$ , with alternating exchange couplings  $J_{p2} \sim 4t_{p2}^2/U = 1100$  K and  $J_{p3} \sim 4t_{p3}^2/U = 220$  K, since the observed magnetic susceptibility<sup>13)</sup> below  $T_{\text{MI}}$  agree well with the calculated susceptibility for the alternating Heisenberg chain with 550 K and 110 K, which is respectively half of the the values  $J_{p2}$  and  $J_{p3}$ , as compared to the one for the Heisenberg chains

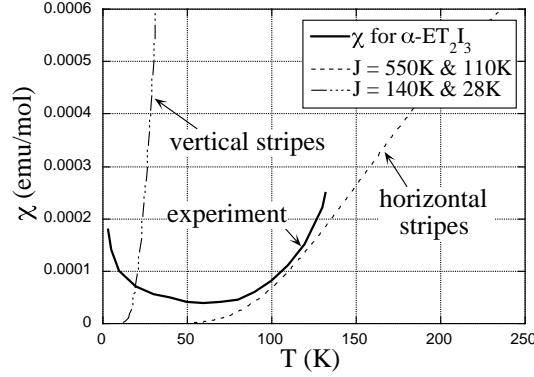


Fig. 26. Calculated magnetic susceptibility<sup>52)</sup> for the Heisenberg chain models and the measured spin susceptibility of  $\alpha$ -(ET) $_2$ I $_3$  taken from ref. 13.

mapped from the CO state with vertical stripes, as shown in Fig. 26.

The effect of applying pressure observed in this compound can be inferred from the results of calculations on the simplified model in §3.4, as follows. The pressure makes the distances of molecules shorter so that the values of transfer integrals increase while it hardly affects the on-site Coulomb energy  $U$ , so the effective on-site Coulomb interaction i.e.  $U/W$  get reduced, where  $W$  denotes the band width. In Figs. 23 and 24, it can be seen that the PM phase is next to the CO phase in the region of smaller  $U/W$ , which is stabilized under high pressure in  $\alpha$ -(ET) $_2$ I $_3$ , as has been discussed by KF.<sup>6)</sup> Although the transport measurements by applying pressure and/or magnetic field have been intensively done in this compound,<sup>12)</sup> experiments on the magnetic properties such as NMR are crucially needed to understand their electronic properties, since in the CO state the charge and the spin degree of freedoms are strongly related to each other. Note that it is difficult to decide whether  $V_{i,j}/W$  increases or decreases by applying pressure to the ET salts since it is natural that the values of  $V_{i,j}$  increase by applying pressure as in the case of the transfer integrals  $t_{i,j}$  and the anisotropy of the ET molecules leads to the difficulty in deducing the values of intersite Coulomb energies  $V_{i,j}$  between ET molecules, although the values of transfer integrals between ETs are carefully calculated by the extended Hückel method for the cases of different configurations.<sup>41)</sup>

As for  $\alpha$ -(ET) $_2$ MHg(SCN) $_4$ , the CO metallic phase found in the calculation for the simplified model in §3.4 may be the candidate for the ground state supporting the existence of a charge disproportionated state proposed by some groups.<sup>16)</sup> However, in §3.3 the results on the calculations for the actual  $\alpha$ MHg-type structure, only insulating states with CO are found to be stable though the band gap for  $V \sim 0.2$  has a quite small value of  $\sim 0.05$  eV in the CO state with vertical stripes as seen in Fig. 19. So at this point incommensurate SDW state due to the nesting of the Fermi

surface, which is not treated in our formulation only considering the states commensurate to the lattice, is the candidate for the ground state as discussed in KF.<sup>5)</sup> To understand their electronic properties, more studies on this series is needed.

#### 4.4 Unified view of $(ET)_2X$

In the work of KF,<sup>6)</sup> a unified view of  $(ET)_2X$  was given as shown in Fig. 27(a), where the two planes are based on Hartree-Fock calculations considering  $\kappa$  and  $\alpha$ -type structures on appropriate Hubbard models. Based on the calculations in §3.4 showing that the inclusion of intersite Coulomb interactions gives rise to a wide region of CO state, their phase diagram can be modified to the one as shown in Fig. 27(b), where the two planes are based on the results in Figs. 20(b) and 23(b). The location of each type of compound is also indicated in Fig. 27(b):  $\kappa$ -phase is in the region of large dimerization where the dimer AF state is stabilized, in contrast with  $\theta_d$ -phase which is located in the region of small dimerization where the CO state is stable.  $\theta$ -phase is located between  $\alpha I_3$  and  $\alpha M\text{Hg}$ -phases on the axis of band overlap. The main difference in the plane of band overlap between Figs. 20(b) and 23(b) is that the  $\alpha M\text{Hg}$ -phase is located in the PM phase far from the CO phase in Fig. 27(a) whereas it is close to the boundary between the CO phase and the PM phase in Fig. 27(b), so the criticality toward the CO phase may play some crucial role, which is beyond the present study.

The effects of pressure are indicated by arrows in Fig. 27(b), following the discussion of Kanoda<sup>8)</sup> and KF<sup>6)</sup> for the  $\kappa$  and  $\alpha$ -phases, and that of H. Mori *et al*<sup>21)</sup> for the  $\theta$  and  $\theta_d$ -phases, respectively. The directions of arrows for the  $\alpha$  and  $\kappa$ -phases are opposite from those for the  $\theta$  and  $\theta_d$ -phases, since in the former compounds it is known that the application of external pressure increases the bandwidth, namely reduces the correlation effect,<sup>6,8)</sup> while in the latter case it widens  $\phi$  and results in the decrease of the bandwidth.<sup>21)</sup> From this point of view, it can be expected that applying pressure to the  $\theta$ -type compounds which is metallic down to low temperature such as  $\theta$ -(ET)<sub>2</sub>I<sub>3</sub> will give birth to an insulating ground state with stripe-type CO state. The effect of uniaxial pressure<sup>54)</sup> is also an intriguing method since it can tune the anisotropy of the system and the stripe-type CO states found in the present study must be highly sensitive to the anisotropy.

There are discussions that in the case of strongly dimerized structures as in the  $\kappa$ -phase the effective on-dimer Coulomb energy can be estimated as  $U_{\text{dimer}} \simeq 2|t_{p1}| + U/2(1 - \sqrt{1 + (4t_{p1}/U)^2})$ , where  $t_{p1}$  is the intradimer transfer integral.<sup>6,8,9)</sup>  $U_{\text{dimer}}$  corresponds to the effective on-site Colomb energy when one maps models of 1/4-filling with strong dimerization to models with 1/2-filled band, *e.g* as has been studied recently for  $\kappa$ -type compounds<sup>55)</sup> for the appropriate 1/2-filled Hubbard model. It can be said that  $U_{\text{dimer}}$  represent the energy scale in the Mott insulating state. On the other hand, as can be seen in Figs. 22 and 25, it appears that the band gap in the CO state increases linearly when  $V$  is increased, which is similarly seen in a classical CO system Fe<sub>3</sub>O<sub>4</sub>.<sup>57,56)</sup> In Fig. 21(b), the line of  $U_{\text{dimer}} = V$  is drawn by the dotted line, which shows qualitative feature similar

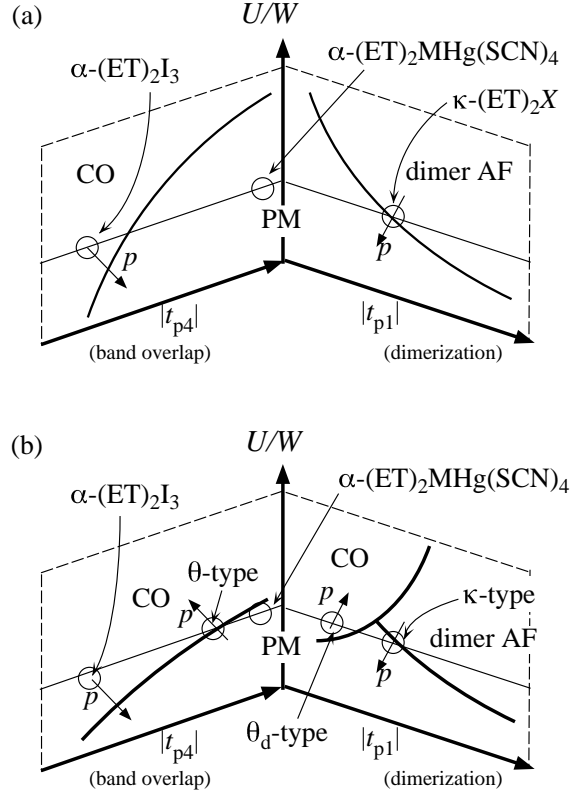


Fig. 27. Schematic phase diagrams for the unified view of  $(\text{ET})_2\text{X}$  in cases of  $V = 0$  (a) by KF<sup>6</sup>) and  $V \neq 0$  (b) by the present work. The notations AF $\kappa$  and AF $\alpha$  are adopted from ref. 6, which represents the AF phases found in their Hartree-Fock calculation on  $\kappa$  and  $\alpha$ -type structures, respectively. PM and CO denotes the paramagnetic metallic and charge ordered phases, respectively. The effect of pressure are shown by arrows.

to the boundary between the CO state and the dimeric AF state in the case of large dimerization  $t_{p1} = 0.30$  eV and in the region of large  $U$ .

## §5. Summary and Conclusion

CO phenomena in 2D organic conductors  $(\text{ET})_2\text{X}$  have been investigated within the Hartree MF approximation on relevant extended Hubbard models including both the on-site and the intersite Coulomb interactions among which the latter are crucial to understand the CO phenomena in 1/4-filled systems. By taking into account the explicit anisotropy of the transfer integrals and the intersite Coulomb interactions for the  $\theta$ ,  $\theta_d$  and  $\alpha$ -type structures, it is found that the intersite Coulomb interactions give rise to stripe-type CO states whose charge patterns are sensitively depending on the parameters of these models.

Based on the results of calculations, implications from the existing experimental facts lead us that



stripes along the bonds with the transfer integral  $t_c$  are realized in  $\theta$ -type compounds, those along  $t_{p4}$  in  $\theta_d$ -type compounds and those along  $t_{p2}$  and  $t_{p3}$  in  $\alpha$ -(ET)<sub>2</sub>I<sub>3</sub>. Their magnetic properties are well reproduced with these stripe-type CO states, considering the effects of quantum fluctuation by mapping the CO states to the  $S = 1/2$  Heisenberg models. A unified view on the electronic states in (ET)<sub>2</sub>X is obtained by taking the degree of dimerization and that of the band overlap as key ingredients, where several states compete to each other, which are the Mott insulating state, the stripe type CO state and the paramagnetic metallic state, realized in the actual compounds.

Such CO states due to intersite Coulomb interaction are expected to be widely realized in other 2D non 1/2-filled (non dimerized) organic compounds showing insulating behavior, *e.g.*  $\alpha'$ ,  $\alpha''$  and  $\beta''$ -phases of (ET)<sub>2</sub>X and also in (ET)<sub>m</sub>X<sub>n</sub> with  $(m, n) \neq (2, 1)$  which do not give 3/4-filled  $\pi$ -band, as well as in non ET compounds.<sup>1, 41)</sup> The present study, which makes a guideline to understand the interrelationship among the experimental facts by taking the CO phenomena as a key factor, might help the understandings of their physical properties.

## Acknowledgements

The author is grateful to Hidetoshi Fukuyama for everyday interactions. He also thanks H. Kohno and H. Yamase for enumerable fruitful suggestions, S. Fujiyama, K. Kanoda, K. Miyagawa, H. Mori, T. Nakamura, Y. Nogami, H. Tajima and T. Takahashi for informative discussions from the experimental point of view, especially K. Kanoda and K. Miyagawa for providing their preprint prior to publication. This work was supported by JSPS Research Fellowships for Young Scientists.

- 
- [1] T. Ishiguro, K. Yamaji and G. Saito: *Organic Superconductors* (Springer 1998) Chap. 5.
  - [2] R. Kato, S. Kagoshima, H. Fukuyama, H. Kino and H. Seo: in *Advances in Synthetic Metals* ed. P. Bernier (Elsevier, Amsterdam, 1999) Chap.4; H. Fukuyama, H. Seo and H. Kino: Proceedings of LT22, Helsinki August 1999 (to appear in Physica B, condmat/9909333).
  - [3] H. Kino and H. Fukuyama: J. Phys. Soc. Jpn. **64** (1995) 1877.
  - [4] H. Kino and H. Fukuyama: J. Phys. Soc. Jpn. **64** (1995) 2726.
  - [5] H. Kino and H. Fukuyama: J. Phys. Soc. Jpn. **64** (1995) 4523.
  - [6] H. Kino and H. Fukuyama: J. Phys. Soc. Jpn. **65** (1996) 2158.
  - [7] K. Oshima, T. Mori, H. Inokuchi, H. Urayama, H. Yamochi and G. Saito: Phys. Rev. B **38** (1998) 938.
  - [8] K. Kanoda: Physica C **282-287** (1997) 299; Hyperfine Int. **104** (1997) 235.
  - [9] R. McKenzie: Science **278** (1997) 820; Comments Cond. Mat. Phys. **18** (1998) 309.
  - [10] Y. Tokura: Kotai Butsuri (Solid State Physics) **28** (1993) 557 [in Japanese].
  - [11] K. Bender, K. Dietz, H. Endres, H. W. Helberg, I. Hennig, H. J. Keller, H. W. Schafer and D. Schweitzer: Mol. Cryst. Liq. Cryst. **107** (1984) 45.
  - [12] K. Kajita, T. Ojio, H. Fujii, Y. Nishio, H. Kobayashi, A. Kobayashi and R. Kato: J. Phys. Soc. Jpn **61** (1992) 23; N. Tajima, M. Tamura, Y. Nishio, K. Kajita and Y. Iye: Synth. Met. **103** (1999) 1958.
  - [13] B. Rothamuel, L. Forro, J. R. Cooper, J. S. Schilling, M. Weger, P. Bele, H. Brunner, D. Schweitzner and H. J. Keller: Phys. Rev. B **34** (1986) 704.

- [14] C. P. Heidmann, A. Barnsteiner, F. Groß-alltag, B. S. Chandrasekhar and E. Hess: Solid State Commun. **84** (1992) 711.
- [15] J. Moldenhauer, Ch. Horn, K. I. Pokhodinia, D. Schweitzer, I. Heiden and H. J. Keller: Synth. Met. **60** (1993) 31.
- [16] K. Miyagawa, A. Kawamoto and K. Kanoda: Phys. Rev. B **56** (1997) 8487; R. McKenzie: cond-mat/9706235; S. Mazumdar, S. Ramasesha, R. Clay and D. Campbell: Phys. Rev. Lett. **82** (1999) 1522.
- [17] H. Mori, S. Tanaka, M. Oshima, G. Saito, T. Mori, Y. Maruyama and H. Inokuchi: Bull. Chem. Soc. Jpn. **63** (1990) 2183; H. Mori, I. Hirabayashi, S. Tanaka, T. Mori, H. Inokuchi, K. Oshima and G. Saito: Synth. Met. **55-57** (1993) 2443; F. L. Pratt, T. Sasaki, N. Toyota and K. Nagamine: Phys. Rev. Lett. **74** (1995) 3892.
- [18] T. Mori, A. Kobayashi, Y. Sasaki, H. Kobayashi, G. Saito and H. Inokuchi: Chem. Lett. **1984** (1984) 957.
- [19] K. Miyagawa, A. Kawamoto and K. Kanoda: preprint.
- [20] R. Chiba, K. Hiraki, H. M. Yamamoto, T. Takahashi and T. Nakamura: private communications.
- [21] H. Mori, S. Tanaka and T. Mori: Phys. Rev. B **57** (1998) 12023; H. Mori, S. Tanaka, T. Mori, A. Kobayashi and H. Kobayashi: Bull. Chem. Soc. Jpn. **71** (1998) 797.
- [22] In ref. 21, the greek character  $\theta$  is used to represent the dihedral angle but here we use  $\phi$  to avoid confusion.
- [23] T. Takahashi and T. Nakamura: private communications.
- [24] H. Kobayashi, R. Kato, A. Kobayashi, Y. Nishio, K. Kajita and W. Sasaki: Chem. Lett. **1986** (1986) 789; *ibid.* **1986** (1986) 833.
- [25] T. Nakamura, R. Kinami, W. Minagawa, T. Takahashi, H. Mori, S. Tanaka and T. Mori: Mol. Cryst. Liq. Cryst. **285** (1996) 57; Synth. Met. **86** (1997) 1991.
- [26] T. Nakamura, W. Minagawa, R. Kinami, Y. Konishi and T. Takahashi: Synth. Met. **103** (1999) 1898.
- [27] T. Komatsu, H. Sato, T. Nakamura, N. Matsukawa, H. Yamochi, G. Saito, M. Kusunoki, K. Sakaguchi and S. Kagoshima: Bull. Chem. Soc. Jpn. **68** (1995) 2233.
- [28] T. G. Takhirov, O. N. Krasochka, O. A. Dyachenko, L. O. Atovmyan, M. Z. Aldoshina, L. M. Goldenberg, R. N. Lyubovskaya, V. A. Merzhanov and R. B. Lyubovskii: Mol. Cryst. Liq. Cryst. **185** (1990) 215.
- [29] J. E. Hirsch and D. J. Scalapino: Phys. Rev. Lett. **50** (1982) 1168; Phys. Rev. B **27** (1983); *ibid.* **29** (1984) 5554; F. Mila and X. Zotos: Europhys. Lett. **24** (1993) 133; K. Penc and F. Mila: Phys. Rev. B **49** (1994) 9670; K. Sano and Y. Ono: J. Phys. Soc. Jpn. **63** (1994) 1250.
- [30] K. Hiraki and K. Kanoda: Phys. Rev. B **54** (1996) 17276; Mol. Cryst. Liq. Cryst. **285** (1996) 157.
- [31] H. Seo and H. Fukuyama: J. Phys. Soc. Jpn. **66** (1997) 1249.
- [32] T. Nakamura, T. Nobutoki, Y. Kobayashi, T. Takahashi and G. Saito: Synth. Met. **70** (1995) 1293; T. Nakamura, R. Kinami, T. Takahashi and G. Saito: Synth. Met. **86** (1997) 2053.
- [33] F. Nad', P. Monceau and J. M. Fabre: Eur. Phys. J. B **3** (1998) 301.
- [34] H. Seo and H. Fukuyama: J. Phys. Soc. Jpn. **67** (1998) 2602.
- [35] H. Seo and H. Fukuyama: J. Phys. Soc. Jpn. **67** (1998) 1848.
- [36] F. Castet, A. Fritsch and L. Ducasse: J. Phys. I France **6** (1996) 583; L. Ducasse, A. Fritsch and F. Castet: Synth. Met. **85** (1997) 1627; A. Fritsch and L. Ducasse: J. Phys. I **1** (1991) 855.
- [37] F. Mila: Phys. Rev. B **52** (1995) 4788.
- [38] H. Mayaffre, P. Weitzek, C. Lenoir, D. Jérôme and P. Batail: Europhys. Lett. **28** (1994) 205.
- [39] J. M. Tranquada, D. J. Buttrey, V. Sachan and J. E. Lorenzo: Phys. Rev. Lett. **73** (1994) 1003; Phys. Rev. B **54** (1996) 12318.
- [40] Signs of the transfer energies are modified in Fig. 4 from those of  $\alpha$ -(ET)<sub>2</sub>NH<sub>4</sub>Hg(SCN)<sub>4</sub>, as  $t_{p3} \rightarrow -t_{p3}$  and  $t_{p4} \rightarrow -t_{p4}$ , in order to compare the features between  $\alpha$ I<sub>3</sub>-type and  $\alpha$ MHg-type. The overall features of the

band structure and the Fermi surface are not changed by this modification.

- [41] T. Mori: Bull. Chem. Soc. Jpn. **71** (1998) 2509; T. Mori, H. Mori and S. Tanaka: *ibid.* **72** (1999) 179; T. Mori: *ibid.* **72** (1999) 2011.
- [42] P. Lambin and J. P. Vigneron: Phys. Rev. B **29** (1984) 3430; H. Kino: Thesis, Tokyo Univ., (1996) p.45.
- [43] P. Thalmeier and P. Fulde: Europhys. Lett. **44** (1998) 242; C. Gros and R. Valenti: Phys. Rev. Lett. **82** (1999) 976.
- [44] H. Seo and H. Fukuyama: J. Phys. Soc. Jpn **66** (1997) 3352.
- [45] D. Poilblanc and T. M. Rice: Phys. Rev. B **39** (1989) 9749; H. J. Schulz: Phys. Rev. Lett. **64** (1990) 1445; M. Kato, K. Machida, H. Nakanishi and M. Fujita: J. Phys. Soc. Jpn. **59** (1990) 1047; T. Giamarchi and C. Lhuillier: Phys. Rev. B **42** (1990) 10641; G. An and J. M. J. van Leeuwen: Phys. Rev. B **44** (1991) 9410.
- [46] H. Tajima: private communications.
- [47] K. Miyagawa and K. Kanoda: private communications.
- [48] Y. Nogami, J. P. Pouget, M. Watanabe, K. Oshima, H. Mori, S. Tanaka and T. Mori: Synth. Met. **103** (1999) 1911; M. Watanabe, Y. Nogami, K. Oshima, H. Mori and S. Tanaka: J. Phys. Soc. Jpn **68** (1999) 2654.
- [49] T. Mori, A. Fuse, H. Mori and S. Tanaka: Physica C **264** (1996) 22.
- [50] In ref. 21, The magnetic susceptibility data was fitted by the 1D as well as 2D Heisenberg model, with exchange coupling  $J = 157$  K and 100 K, respectively. Here only the 1D case is considered since our MF calculation suggests the 1D ordering of charges.
- [51] H. Yamase, H. Kohno, H. Fukuyama and M. Ogata: J. Phys. Soc. Jpn. **68** (1999) 1082 J. M. Tranquada, B. J. Sternlieb, J. D. Axe, Y. Nakamura and S. Uchida: Nature (London) **375** (1995) 561.
- [52] L. N. Bulaevskii: Sov. Phys. JETP **17** (1963) 684; Sov. Phys. Solid State **11** (1969) 921.
- [53] H. Kuwahara, Y. Tomioka, A. Asamitsu, Y. Moritomo and Y. Tokura: Science **270** (1995) 961; Y. Moritomo, A. Asamitsu, H. Kuwahara and Y. Tokura: Nature (London) **380** (1996) 141.
- [54] M. Maesato, Y. Kaga, R. Kondo and S. Kagoshima: to appear in Rev. Sci. Instrum.
- [55] H. Kino and H. Kontani: J. Phys. Soc. Jpn. **67** (1998) 3691; H. Kondo and T. Moriya: J. Phys. Soc. Jpn. **67** (1998) 3695; K. Kuroki and H. Aoki: Phys. Rev. B **60** (1999) 3060.
- [56] V. I. Anisimov, I. S. Elfimov, N. Hamada and K. Terakura: Phys. Rev. B **54** (1996) 4387.
- [57] S. K. Park, T. Ishikawa and Y. Tokura: Phys. Rev. Lett. **58** (1998) 3717.